Engineering Geology 366 (2026) 108671

Contents lists available at ScienceDirect

Engineering Geology

journal homepage: www.elsevier.com/locate/enggeo

Beyond critical state: A critical-state hydrodynamic model (CSHM) for solid-fluid phase transition of clay

Hang Feng [a,b], Zhen-Yu Yin [a,b,*], Wei Cheng [a,b]

[a] Department of Civil and Environmental Engineering, The Hong Kong Polytechnic University, Hong Kong, China
[b] Research Institute for Land and Space, The Hong Kong Polytechnic University, Hong Kong, China

ARTICLE INFO

Keywords:
Constitutive model
Clay
Quasi-static stress
Viscous stress
Rheology
Elastoplasticity

ABSTRACT

Clay's solid-fluid phase transition, a key cause of geohazards like landslides and debris flows, remains notoriously difficult to model due to its coupled frictional yielding and strain-rate-dependent fluidization. Its complexity poses a substantial challenge to constitutive modeling. For the first time, this study proposes a novel critical-state hydrodynamic model (CSHM), which efficiently captures clay's nonlinear solid-fluid phase transition by integrating quasi-static and viscous stress components in a unified framework. The quasi-static stress is described by a critical-state-based elastoplastic model, representing the solid-like behavior. In contrast, the viscous stress is described using a novel hydrodynamics-based rheological model that captures the fluid-like behavior by introducing a state variable termed "clay temperature". The quasi-static component captures key aspects including nonlinear elasticity, stress dilatancy, and critical state, whereas the proposed viscous component describes shear-heating or shear-cooling rheology. Subsequently, extensive element simulations are employed to evaluate the new CSHM. Finally, validation against experimental data demonstrates that the CSHM accurately captures the clay's solid-to-fluid phase transition. The analyses reveal that: (i) While sand undergoes a shear-induced heating phase transition and is well described by the existing kinetic theory, clay exhibits shear-cooling, which our novel model accurately captures. (ii) Clay's phase transition is characterized by two transitional points (critical-state point and viscous-stress-dominant point) and three different regimes (solid-like, transitional, and fluid-like). (iii) Unlike the traditional HB model, a 2D model describing stress in the fluid-like state, the CSHM is a 3D full-range phase transition model that captures evolution from initial to critical state, and eventually fluid-like state.

1. Introduction

The phase transition phenomena have been observed in many natural systems, including ice melting (Fig. 1a), flow-like landslides, and debris flows (Fig. 1b). Ice melting, a well-studied phase transition of water in thermodynamics, occurs when the solid structure of ice breaks down into a fluid phase as thermal energy (temperature) increase. In contrast, debris flows, among the most dangerous geological events (Li et al., 2019), exhibit nonlinear solid-to-fluid transitions where soils transition from a solid-like state to a fluid-like state (Wang et al., 2024). A representative case is the landslide on the Meida Highway in Meizhou City, China, on May 1, 2024. Initially, the soil exhibited solid-like behavior, supporting the highway. However, the yielding of effective stress triggered a transition to fluid-like flow, ultimately causing the catastrophic failure that resulted in 48 fatalities and 30 injuries (Xue et al., 2025) (Fig. 1b). In addition, numerous flow-like landslides that pose a big threat to man-made structures have been reported (e.g., Liu et al., 2022; Shen et al., 2024; Su et al., 2024). These events underscore the vital need to accurately model the solid-fluid phase transition in soils for the analysis of landslides in engineering geology.

Accurately describing the soil's phase transition remains a significant challenge due to its inherent multidiscipline complexity. In physics, Nobel Laureate De Gennes (1992) first classified materials similar to soils, behaving both solid- and fluid-like behavior, as soft matter. Liu and Nagel (1998) introduced a possible phase transition space, suggesting that the phase transition of the soft matter is governed by factors such as concentration, stress, or "temperature" (an analog of thermal temperature) (see Fig. 1c). Subsequent studies attempted to complete this phase transition space. Many studies on granular media defined "granular temperature" via shear strain rate and demonstrated that the increasing "granular temperature" (i.e., shear strain rate) can induce the transition of soils from solid- to fluid-like states (Goldhirsch, 2003; Jiang and Liu,

* Corresponding author.
E-mail addresses: 23039257r@connect.polyu.hk (H. Feng), zhenyu.yin@polyu.edu.hk (Z.-Y. Yin), w1cheng@polyu.edu.hk (W. Cheng).

https://doi.org/10.1016/j.enggeo.2026.108671
Received 15 September 2025; Received in revised form 7 December 2025; Accepted 9 March 2026
Available online 12 March 2026

2009; Luding et al., 2021). However, a rational phase transition space for clays is still unclear.

The engineering field usually examines the macroscopic stress evolution from different disciplines: (i) Soil mechanics: Traditional soil mechanics usually employs solid mechanics principles under small-strain and small-strain-rate regimes (typically$<1\ s^{-1}$), characterized complex elastoplasticity (e.g., nonlinear elasticity and friction-yielding characteristics). The critical state theory (Wood, 1990) states that soils under sustained shearing will reach the critical state, where the shear stress, mean stress, and volume will no longer increase under continued deformation. However, this theory ignores the strain-rate effect (i.e., a term that may be related to "soil temperature"). While rate-dependent phenomena like creep and stress relaxation have been incorporated in Elastic Visco-Plastic (EVP) models (e.g., Yin et al., 2020; Cheng and Yin, 2024), these models remain limited to strain rates $\leq 1\ s^{-1}$, failing to capture fluid-like responses at higher rates (see Fig. 2(a)). Consequently, classical soil mechanics only describes behavior from the initial state to the critical state, effectively addressing solid-like responses. (ii) Fluid mechanics: Traditional fluid mechanics addresses the large-strain-rate regime (typically$>10\ s^{-1}$), where viscous rheological properties such as shear-thinning or shear-thickening dominate (Meshkati et al., 2021). Forterre and Pouliquen (2008) systematically characterized granular behavior in this regime (Fig. 2b), revealing that the ratio of shear stress to mean stress deviates from a constant with increasing strain rates, approaching a fluid-like value. However, fluid mechanics frameworks fail to describe solid-like responses at small strains, such as elastoplasticity or frictional yielding. Consequently, classical fluid mechanics only captures behavior at the fluid-like regime, neglecting behavior between the initial and critical states.

The above complexity has resulted in a critical challenge of establishing a unified solid-fluid phase transition model across the full range of strain rates. Accordingly, this study focuses on developing the solid-fluid phase transition model across small to large strain-shear-rate regimes, distinct from "soil liquefaction" in geotechnics. Traditional liquefaction, a special solid-like response, describes the reduction of rate-independent solid-like effective stress to zero (e.g., due to the void ratio change of sands or the destruction of clays). Note that the time-dependent soil behaviors at solid-like state (e.g., creep, stress relaxation) are ignored in this study.

Developing robust solid-fluid phase transition constitutive models must satisfy two main requirements: (i) capturing the multifaceted responses from both soil mechanics and fluid dynamics within a unified framework; and (ii) seamlessly bridging solid-like and fluid-like behaviors across different strain-rate regimes (Feng et al., 2025).

To satisfy these requirements, various models have been developed, including two main types: sands and clays. Among these models, the critical-state-based stress superposition framework (i.e., decomposing the total effective stress into rate-independent solid-like and rate-dependent fluid-like stresses) is particularly favored for its conceptual simplicity, mechanistic transparency, and ability to seamlessly integrate solid- and fluid-like behaviors. In this framework, the critical state point in soil mechanics, analogous to the jamming point in jamming transition, serves as a criterion for distinguishing solid-like and fluid-like states during the intricate phase transition (see Fig. 2 (b)) (see Feng et al., 2025). This study will explore this framework in detail.

Compared to clays, models for the phase transition of sands have been extensively developed (e.g., Vescovi et al., 2013; Baumgarten and Kamrin, 2019). In these models, total stress comprises a rate-independent frictional component (quasi-static, solid-like) and a rate-dependent collisional component (viscous, fluid-like), as shown in Fig. 3. When quasi-static stress predominates, the material exhibits a solid-like state, whereas the dominance of viscous stress indicates a fluid-like state. Specifically, quasi-static stress is described with an elastoplastic relation with the critical state, while viscous stress uses a kinetic theory (Garzó and Dufty, 1999). The critical state in the quasi-static component represents the failure of solid-like stress and marks the initiation of the phase transition (Feng et al., 2025). Kinetic theory quantifies sand's viscous stress via granular temperature, a parameter analogous to thermodynamic temperature observed in water phase transitions, thereby enabling a continuous shift between solid-like and fluid-like states (Goldhirsch, 2003) (see Fig. 1c).

For the phase transition of clays, only a limited number of studies have attempted to establish effective models (Prime et al., 2014a, 2014b; Chen, 2020). Prime et al. (2014a, 2014b) introduced a model

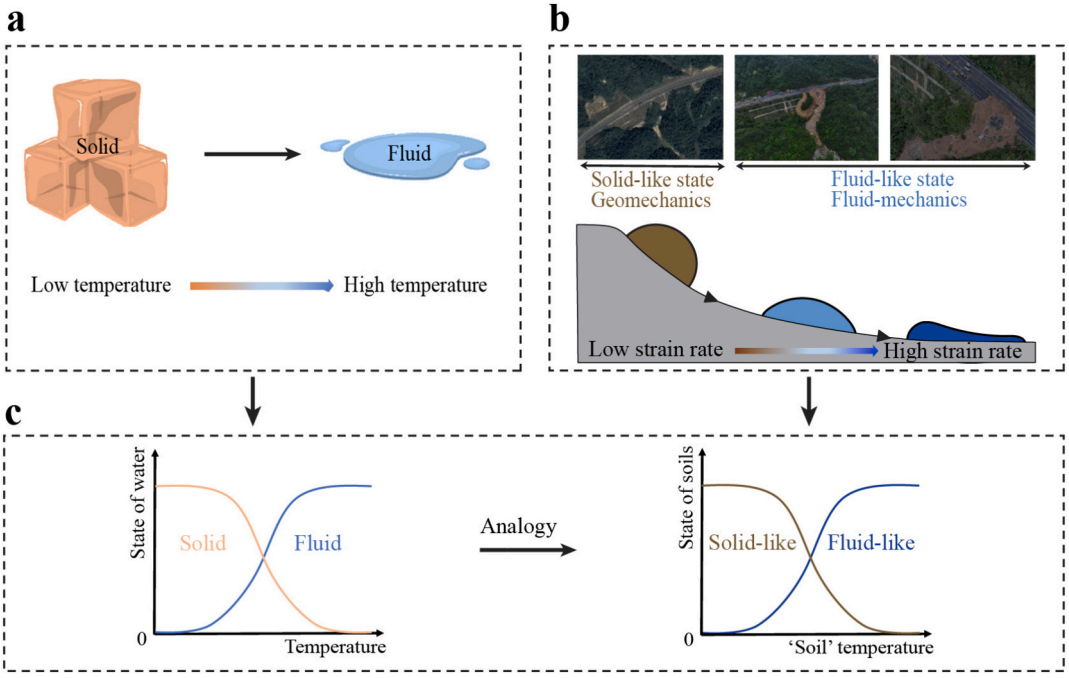

Fig. 1. Phase transition phenomena. (a) Phase transition of water. (b) Phase transition of soils in debris flows (Xue et al., 2025). (c) Possible solid-fluid phase transition mechanism for soils in analog with water (Raz and Levine, 2023).

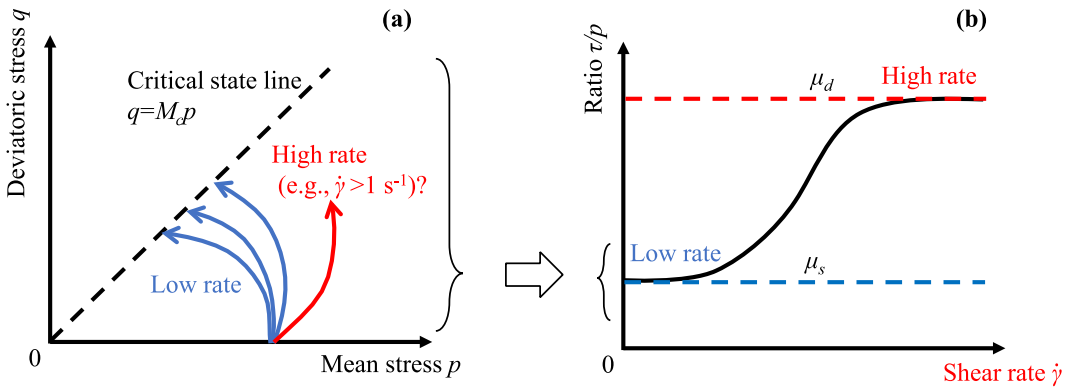

Fig. 2. Soil response from different disciplines (undrained shear test). (a) Critical state theory in soil mechanics at solid-like state. (b) Rheology theory in fluid mechanics at fluid-like state.

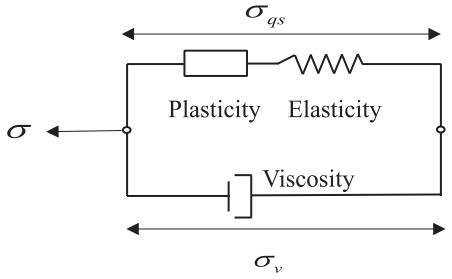

Fig. 3. Basic framework for the solid-to-fluid phase transition model of soils.

that combines elastoplasticity with Bingham-type rheology, where the change from solid- to fluid-like characteristics is governed by the loss of second-order work stability (Hill, 1958). Although innovative, this approach treats clays as either fully solid-like or fluid-like throughout the whole process and overlooks the coexistence of these behaviors. Furthermore, the abrupt activation of viscous stress upon the violation of second-order work introduces stress discontinuity, resulting in a non-smooth transition between solid-like and fluid-like states. Chen (2020) proposed a model for clay's phase transition via the stress superposition framework, i.e., decomposing total stress into inter-aggregate (solid-dominated) and intra-aggregate (fluid-dominated) components. While conceptually novel, this model lacks explicit equations. To the authors' knowledge, a phase transition model for clays that seamlessly bridges solid-like and fluid-like behaviors has yet to be developed.

To address these gaps, this study builds on a framework analogous to Feng et al. (2025)'s sand model to propose a Critical-State-based Hydrodynamic Model (CSHM) for capturing the phase transition dynamics of clay, a phenomenon previously unexplored. The model decomposes the total effective stress into quasi-static and viscous components. The quasi-static component is described using a critical-state-based elasto-plastic clay model, while the viscous component is governed by a new phenomenological hydrodynamic model introducing "clay temperature" as a key state variable. The proposed CSHM is also extensively evaluated using element simulations and rigorously validated through comparisons with comprehensive experimental data. The proposed model is designed to facilitate the precise analysis and prediction of geohazards, particularly flow-like landslides in the field of engineering geology (e.g., Yang et al., 2024; Ye et al., 2024; Urmi et al., 2024).

The paper is organized as follows: Section 2 discusses the fundamental behaviors of clays observed in laboratory element tests, from soil mechanics to fluid mechanics. Section 3 presents the proposed CSHM, while Section 4 discusses the model parameters and implementation. The evaluation of CSHM is provided in Section 5. Section 6 further validates the model through simulations of experimental data, followed by a discussion of the model in Section 7. Finally, Section 8 summarizes the main conclusions.

2. Behaviors of clays: from soil mechanics to fluid mechanics

2.1. Solid-like behaviors in soil mechanics

Common element tests in soil mechanics include the triaxial test, oedometer compression test, plane strain test, and simple shear test. Except for the simple shear test, these tests are constrained by limited deformation. Nevertheless, they have provided extensive data for describing solid-like responses and developing effective constitutive models in soil mechanics (Wood, 1990; Lade, 2005; Yin et al., 2020). In particular, key features of clay in soil mechanics are revealed: (i) compressive characteristics, e.g., the stiffness of clay increases with pressure during the isotropic compression test; (ii) frictional characteristics, e.g., shear stress rises with increasing pressure until the failure stage during the triaxial test and simple shear test; and (iii) shear-dilatancy, where volumetric strain is influenced by shear stress. Other observed features include small strain stiffness, anisotropy, cyclic loading, rate effects, and temperature effects. Given the strain rate in the geotechnical experiments (e.g., creep) is no more than 1 s^{-1}, smaller than strain rates in fluid mechanics, this study specifically focuses on the three basic rate-independent features during the solid-like state. Other features can be incorporated into the proposed model in future research (see discussion in Section 7).

2.2. Fluid-like behaviors in fluid mechanics

To investigate the fluid-like behavior of clays under large deformations, laboratory tests such as viscometers and rheometers are commonly used to measure clay rheology (see Fig. 4). The rotational viscometer (Fig. 4(a)) in fluid mechanics is similar to the vane shear test in geotechnics, which evaluates the undrained shear strength of clays. However, the vane shear cannot measure shear rate, and the viscometer is limited to constant viscosity measurements, unable to consider varying viscosity (Boukpeti et al., 2012). Thus, neither the vane shear nor the viscometer qualifies as an element test.

In contrast, the rheometer, including the concentric cylinder, plate-plate, and cone-plate types, effectively addresses the limitations of viscometers. The widely used plate-plate rheometer serves as an example for a brief discussion (see Fig. 4(b)). In this test, the material is placed between a stationary lower plate and a rotating upper plate. The shearing process in a rheometer involves several key conditions: (i) The sample is confined to a small size, with a height of 1–5 mm and a diameter of 25–50 mm, effectively approximating laminar flow and uniform deformation. (ii) Force analysis indicates that the sample can be described using the simple shear test (see Fig. 4(c)). (iii) With a constant distance between the plates and rapid test duration, the constant volume

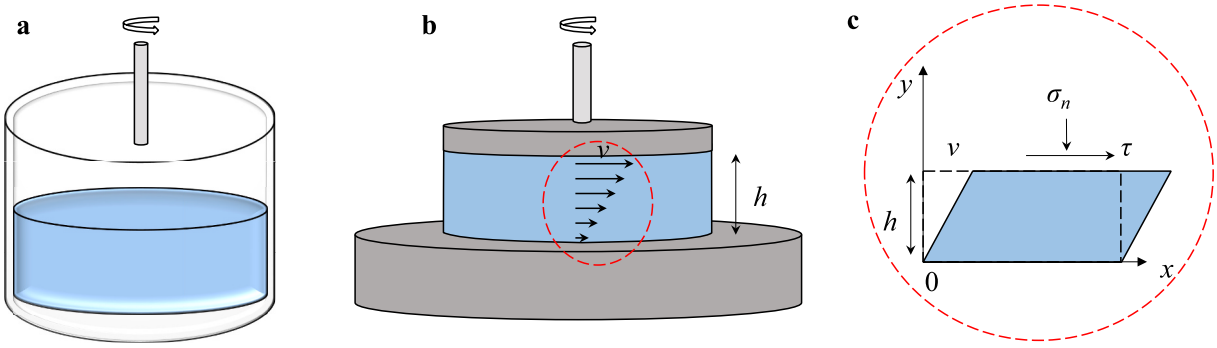

Fig. 4. Experiments in fluid mechanics. (a) The viscometer; (b) The rheometer; (c) Simple shear test.

condition is maintained, akin to the undrained test in soil mechanics. (iv) Measuring vertical stress in the rheometer is challenging. (v) The sample is prepared using saturated remolded mud, allowing it to be considered as normally consolidated clay. Thus, the rheometer test can be approximated as a simple shear test of normally consolidated clay under constant volume conditions, which cannot provide the vertical stress. To obtain results for vertical stress, one should measure vertical stress in the rheometer or use numerical simulations such as discrete element modeling (DEM). However, to the present author's knowledge, these approaches have not yet been employed to investigate the simple shear condition of clay at large shear rates.

Using the rheometers, many studies have measured the shear rate-shear stress curves of clay (e.g., Yi et al., 2018; Liu et al., 2023; Wei et al., 2025). Fig. 5 shows the experimental data from Yi et al. (2018) and Wei et al. (2025), which were obtained using plate-plate rheometers. Yi et al. (2018) tested Malaysian kaolin clay across shear rates of 10^{-1} to 10^{2} at water contents of 72%, 83%, and 87%. In contrast, Wei et al. (2025) investigated natural kaolin clay over a narrower shear rate range from 10^{-1} to 10^{1} and lower water contents at 40%, 49%, and 59%. As shown in Fig. 5, the shear stress-shear strain rate curves exhibit two distinct stages demarcated by the critical shear stress τ_s (yielding stress). Below a threshold shear rate regime (i.e., 10^{0}–10^{1} s^{-1} in Fig. 5(a) and 10^{-1}-10^{0} s^{-1} in Fig. 5(b)), the shear stress plateaus at τ_s. This stage can be seen as a typical solid-like behavior. Beyond this critical state, shear stress increases significantly with shear rate, dominated by fluid-like rheological behavior. Notably, the yielding stress exhibits significant variation across clay types. Fig. 5 also demonstrates the reduction in shear stress with increasing water content. This behavior can be explained by two mechanisms: (i) Lower water content correlates with smaller initial mean stress under simple shear conditions, thereby lowering the yield stress. (ii) The increase of water content progressively transitions the clay from a solid to semi-solid, plastic, and ultimately fluid-like states. In this study, distinct water contents are assumed to map to specific mean stresses derived from isotropic compressive curves, providing a mechanistic basis for studying solid-fluid transitions.

Fig. 6 presents a re-interpretation of the data from Fig. 5, showing viscous stress (total shear stress minus solid-like stress τ_s) plotted against the shear rate. Both datasets exhibit a linear relationship between viscous stress and shear rate in logarithmic plane. Fig.6(a) shows the water content does not influence this relation while the water content can influence Fig.6(b). The qualitative discrepancies between Fig. 6(a) and 6(b) could be described as the different types of clays employed. Fig. 6(a) features Malaysian kaolin tested at water contents near its liquid limit (W_L = 80%), displaying water content-independent behavior. Fig. 6(b) employs natural kaolin with a liquid limit of 39.5%, where two samples near W_L exhibit similar independence, while a sample largely exceeding W_L shows water content dependence. These observations suggest the liquid limit may emerge as a critical factor governing state-dependent rheological behavior. Specifically, samples near the liquid limit may display invariant viscous stress responses, whereas deviations above W_L may introduce water content sensitivity. This mechanistic distinction warrants further investigation to understand the influence of water content.

3. Critical-state hydrodynamic model (CSHM)

This section attempts to establish a simple but robust model seamlessly bridges solid- and fluid-like responses discussed in Section 2. It commences with an overview of the basic assumptions and theoretical structure, followed by a description of the critical-state-based quasi-static stress and the hydrodynamics-based viscous stress. The summary of the CSHM is finally given.

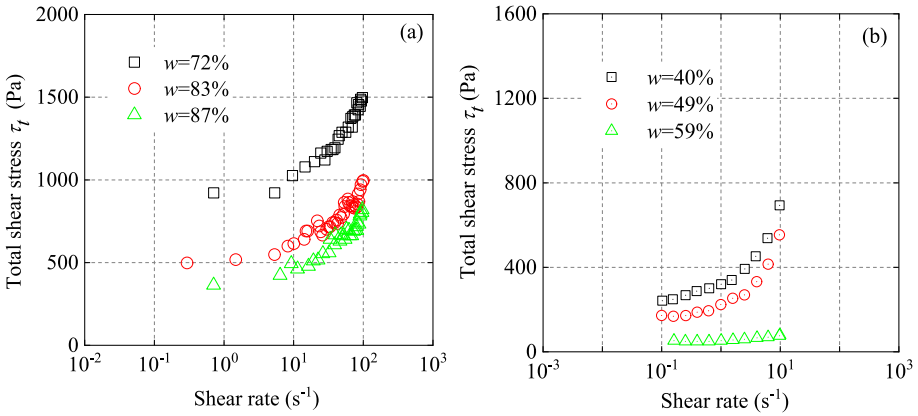

Fig. 5. The shear stress and shear rate from the rheometer test. (a) Experimental results with a large shear rate range from 10^{-1} to 10^{2} s^{-1} (Yi et al., 2018). (b) Experimental results with a small shear rate range from 10^{-1} to 10^{1} s^{-1} (Wei et al., 2025).

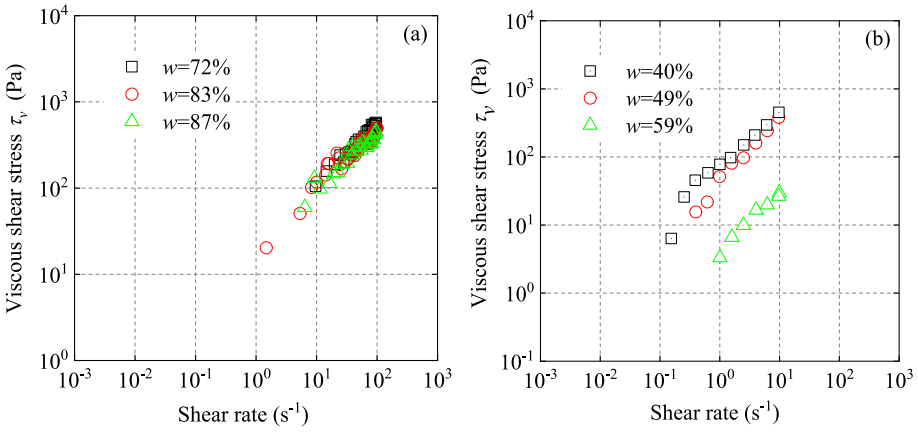

Fig. 6. Development of the fluid-like stress with the shear rate. (a) Experimental results by Yi et al. (2018). (b) Experimental results by Wei et al. (2025).

3.1. Basic assumptions and framework

Prior to introducing the specific formulations, we first clarify the underlying assumptions:

AS-1: The clay is modeled as a homogeneous saturated medium governed by Terzaghi's effective stress principle.

AS-2: Analogous to the behavior of sand (Prime et al., 2014b; Redaelli et al., 2016; Wu et al., 2020), the stress superposition framework is also applicable to clay, wherein the mechanical response is governed by both solid-like and fluid-like stress components. The former is modeled using elastoplastic theory to capture friction-induced yielding, and the latter with a strain-rate-dependent hydrodynamic model. Note that this assumption is supported by the deformation mechanisms of clay outlined in Appendix A and has also been adopted in previous studies (Prime et al., 2014a, 2014b; Chen, 2020). It is acknowledged that a clear physical mechanism governing clay's phase transition remains to be fully revealed in existing literature. Consequently, the stress decomposition concept is necessarily treated as a theoretical assumption in this study. This assumption, however, allows us to construct a robust constitutive framework that effectively models the complex phase transition behavior of clay.

AS-3: This study assumes that the clay exhibits incompressible behavior upon transitioning to the fluid-like state, i.e., the clay keeps the constant volume once reaching the critical state. Note that this assumption is also employed by the widely-used the $\mu(I)$ rheology model (GDR-MiDi, 2004; Jop et al., 2006; Forterre and Pouliquen, 2008), and other models (Baumgarten and Kamrin, 2019).

AS-4: This study does not consider traditional soil liquefaction, a special solid-like response that involves the reduction of rate-independent effective stress to zero, which may occur from the destruction of clay fabrics.

AS-5: This study assumes that the solid-like stress is rate-independent. Accordingly, the model excludes time-dependent solid-like behaviors such as creep and stress relaxation, and the critical state line (CSL) is considered invariant with strain rate. The justification for this simplification is provided in Section 7.

Based on the above assumptions, we can now establish the framework for the phase transition of clays. First, in accordance with Terzaghi's effective stress principle (i.e., AS-1), we decompose the total Cauchy stress tensor $\boldsymbol{\sigma}$ for saturated clay into effective solid-phase stress $\boldsymbol{\sigma}_s$ and fluid-phase stress $\boldsymbol{\sigma}_f$ (see Eq. (1)). The fluid stress is expressed via $\boldsymbol{\sigma}_f = \boldsymbol{s}_f + p_f\mathrm{I}$ (where $\boldsymbol{s}_f$ is the deviatoric stress tensor, representing the fluid's viscous effect; $p_f\mathbf{I}$ is the isotropic stress tensor, controlled by the pore pressure). Considering that the shear resistance provided by the fluid is orders of magnitude smaller than that of the soil skeleton during undrained shear, we ignore the deviatoric component of the fluid stress.

$$\boldsymbol{\sigma} = \boldsymbol{\sigma}_s + \boldsymbol{\sigma}_f \tag{1}$$

Second, based on the stress superposition concept (i.e., AS-2), the effective solid-phase stress of saturated clay is decomposed into two components (see Eq. (2)): the quasi-static stress $\boldsymbol{\sigma}_{qs}$ and viscous stress $\boldsymbol{\sigma}_v$:

$$\boldsymbol{\sigma}_s = \boldsymbol{\sigma}_{qs} + \boldsymbol{\sigma}_v \tag{2}$$

where $\boldsymbol{\sigma}_{qs}$ is the quasi-static stress, which is described by a rate-independent critical-state elastoplastic model; $\boldsymbol{\sigma}_v$ is the viscous stress, which is described by a proposed hydrodynamic model using "clay temperature", mirroring "granular temperature" in the kinetic theory, to quantify fluid-like responses. Details are in Sections 3.2 and 3.3.

3.2. Elastoplastic critical-state-based model for quasi-static stress

Following the framework and assumptions (i.e., AS-5), a rate-independent elastoplastic constitutive relation grounded in the critical state concept is applied to describe the solid-like behavior of clays. Using classical critical state theory (Schofield and Wroth, 1968), clays at critical state attain time-invariant quasi-static stress and volume under prolonged shear strain, indicating clays change from a solid state to a fluid state. While various advanced critical-state-based elastoplastic models exist that capture intricate soil behaviors (e.g., anisotropy, small-strain stiffness), this study focuses on establishing a simplified yet robust phase transition model. To this end, the framework of the Modified Cam Clay (MCC) model is selected for its balance of theoretical clarity and practical applicability.

Following the elastoplastic theory, the strain increment has two parts: an elastic part $d\boldsymbol{\varepsilon}^e$ and a plastic part $d\boldsymbol{\varepsilon}^p$, given as follows:

$$d\boldsymbol{\varepsilon} = d\boldsymbol{\varepsilon}^e + d\boldsymbol{\varepsilon}^p \tag{3}$$

where $d\boldsymbol{\varepsilon}^e$ and $d\boldsymbol{\varepsilon}^p$ are the elastic and plastic strain increments, respectively. The elastic and plastic responses are described as follows:

i) Nonlinear elastic behavior.

The quasi-static stress increment is calculated using the elastic strain increment $d\boldsymbol{\varepsilon}^e$:

$$d\boldsymbol{\sigma}_{qs} = \mathbf{D}^e_{qs} : d\boldsymbol{\varepsilon}^e \tag{4}$$

where $\mathbf{D}^e_{qs}$ denotes the fourth-order elastic stiffness tensor, formulated as a function of the volumetric elastic modulus K_{qs} and Poisson's ratio ν. The modulus K_{qs} is derived experimentally from the compressive curve of laboratory tests, given as follows:

$$K_{qs} = \frac{1+e_0}{\kappa} p_{qs} \tag{5}$$

where e_0 is the initial void ratio; κ is the swelling index in the

compressive curve; p_{qs} is the quasi-static isotropic stress.

ii) Plastic behavior (stress dilatancy and critical state concept).

The plastic behavior can be determined by the yield criterion, hardening rule, and flow rule.

In our model, the associated flow rule is assumed, i.e., the flow rule is the same as the yield criterion. The yield function is given as follows:

$$f = \frac{q_{qs}^2}{M_c^2} + p_{qs}^2 - p_{qs}p_c \tag{6}$$

where M_c is the slope of the CSL; p_{qs} and q_{qs} are the isotropic and deviatoric stresses, respectively. p_c is the hardening parameter, controlled by the hardening rule:

$$dp_c = p_c\left(\frac{1+e_0}{\lambda-\kappa}\right)d\varepsilon_v^p \tag{7}$$

where $d\varepsilon_v^p$ is the volumetric plastic strain increment.

The above three-dimensional equations can generate the corresponding isotropic stress (p_{qs}) and deviatoric stress (q_{qs}) components. Under simple shear conditions (see Appendix B), the simplified quasi-static stress can be subsequently obtained. As shown in Eq. (8), the vertical and shear stresses are related to p_{qs} and q_{qs}. Meanwhile, key parameters governing the quasi-static stress are presented in Table 1.

$$\boldsymbol{\sigma}_{2D,qs} = \begin{bmatrix} \sigma_{n,qs} \\ \tau_{qs} \end{bmatrix} = \begin{bmatrix} p_{qs} \\ q_{qs}/\sqrt{3} \end{bmatrix} \tag{8}$$

where p_{qs} and q_{qs} are the quasi-static isotropic stress and quasi-static deviatoric stress, respectively; $\boldsymbol{\sigma}_{2D,qs}$ is the simplified quasi-static stress vector under simple shear test; $\sigma_{n,qs}$ and τ_{qs} are the quasi-static vertical stress and quasi-static shear stress under simple shear test, respectively.

3.3. Phenomenological hydrodynamics-based model for viscous stress

This section develops a hydrodynamic framework for viscous stress of clayey soils. First, we briefly discuss the well-established kinetic-theory-based hydrodynamics model for viscous stress of sands. Then, based on this model, we propose a new hydrodynamic formulation for clayed soils.

The rheological behavior of sands has been extensively studied since Bagnold's pioneering work (Bagnold, 1954). Subsequent research efforts have advanced two primary types: (i) theoretical frameworks, such as kinetic-theory-based hydrodynamic models (Jenkins and Savage, 1983; Savage, 1998; Garzó and Dufty, 1999; Lun, 2000; Goldhirsch, 2003), and (ii) phenomenological frameworks, including the $\mu(I)$ model established via experimental investigations (Forterre and Pouliquen, 2008). In the former model, the viscous stress is obtained by considering the collisional mechanism, which is expressed as follows:

$$\boldsymbol{\sigma}_v = p_v\mathbf{I} - 2\eta_v\left(\dot{\boldsymbol{\epsilon}} - \frac{1}{3}(\nabla\cdot\mathbf{u})\mathbf{I}\right) - \gamma_v(\nabla\cdot\mathbf{u})\mathbf{I} \tag{9}$$

where $\dot{\boldsymbol{\epsilon}}$ represents the strain rate tensor; $\mathbf{I}$ is the identity tensor; p_v, η_v, and γ_v stand for the viscous mean stress, shear viscosity, and bulk viscosity, respectively.

In the kinetic theory, the granular temperature T_g, shear viscosity η_g, and viscous shear stress τ_g in the simple shear test conditions are expressed as follows (the derivation process refer to Feng and Yin (2025)):

$$T_g \sim d^2\dot{\gamma}^2 \tag{10}$$

$$\eta_g \sim \rho d T_g^{0.5} \sim \rho d^2\dot{\gamma} \tag{11}$$

$$\tau_g \sim \rho d^2\dot{\gamma}^2 \tag{12}$$

where $\dot{\gamma}$ is the shear rate under simple shear conditions.

Remark 1. Can the kinetic-theory-based hydrodynamic model presented above accurately describe the fluid-like viscous stress behavior of clay? To address this question, we compare experimental viscosity data of clay (e.g., as provided in Subsection 2.2 of Yi et al., 2018) with numerical results obtained from the kinetic-theory-based model. A comparison of these data is presented in Fig. 7. The results indicate that the viscosity of clay decreases with increasing shear rate, whereas the granular viscosity predicted by the kinetic-theory-based hydrodynamic model increases with shear rate, a trend explicitly captured by the positive correlation described in Eq. (12). Therefore, based on this comparison, it can be concluded that the current kinetic-theory-based hydrodynamic model is not suitable for characterizing the fluid-like stress of clay.

Based on the discussion in **Remark 1**, a novel hydrodynamic stress model tailored for clay should be developed, and the existing kinetic-theory-based framework originally proposed for sand requires significant modification. While a model for clay could, in principle, be derived directly from the energy balance framework, this approach yields a stress equation structurally similar to that of sand (Eq. (11) and (12)). Consequently, we propose an alternative strategy: we adapt the theoretical hydrodynamic framework into a phenomenological model for clay through three key modifications:

i) 3D hydrodynamic-based stress equation.

First, we retain the core constitutive structure (i.e., Eq. (9)) but replace the "granular temperature" with a newly defined "clay temperature". This concept provides a physical description of the viscous stress in clay systems, effectively describing the Liu-Nagel phase transition space and enabling the development of a three-dimensional constitutive model. Accordingly, the viscous stress tensor of clay is expressed through a hydrodynamic formulation given by Eq. (13). The

Table 1
Parameters in the proposed CSHM.

Stress	Parameters	Definition	Values			
			Simulation	Montmorillonite	Natural kaolin	Malaysian kaolin
Quasi-static	e_0	Initial void ratio	0.60	–	1.79, 1.54, 1.28	1.87, 2.16, 2.26
	ν	Poisson's ratio	0.20	–	0.33	0.33
	κ	Swelling index	0.02	–	0.053	0.053
	λ	Compression index	0.08	–	0.244	0.244
	M_c	The slope of CSL	1.20	–	0.90	0.90
Viscous	n	Viscous coefficient	−0.30, 0.00, 0.30	−0.5	−0.30	−0.51
	m_c	Viscous coefficient	0.005, 0.025, 0.100	0.007, 0.0065, 0.004	0.003, 0.325, 0.044	0.0275, 0.0225, 0.021
	ρ	Dry density (kg/m^3)	1000	2000	2000	2000
	d	Representative diameter (m)	1.00	1.00	1.00	1.00
	μ_v	Viscous friction coefficient	1.00	–	–	–

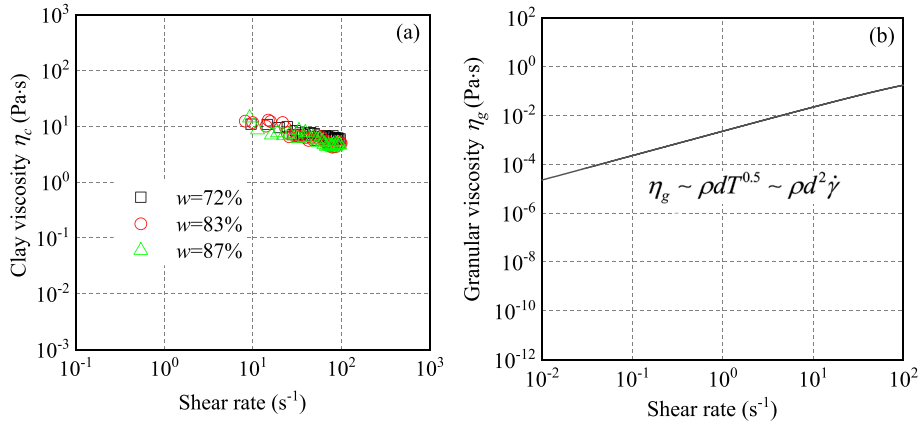

Fig. 7. Comparison between experimental clay's viscosity and numerical sand's viscosity. (a) Experimental clay's viscosity from Yi et al. (2018); (b) Numerical sand's viscosity from the kinetic-theory-based hydrodynamic model (parameter from Feng et al., 2025).

current formulation deviates from the model in Eq. (9) by deliberately omitting the bulk viscosity term. While the original kinetic-theory model (Eq. (9)) accounts for compressibility, the proposed model for clay (Eq. (13)) assumes incompressibility (i.e., AS-3 in Section 3.1).

$$\boldsymbol{\sigma}_v = p_v \mathbf{I} - 2\eta_v \dot{\boldsymbol{\varepsilon}} \tag{13}$$

where $\dot{\boldsymbol{\varepsilon}}$ represents the strain rate tensor; p_v and η_v are the viscous mean stress and shear viscosity, respectively.

In the kinetic-theory-based hydrodynamic model (see Appendix C), both the viscous hydrostatic stress and shear viscosity are governed by the granular temperature T_g. Given that the classical granular temperature T_g is fundamentally unsuitable for clay (see Remark 1), the proposed model for clay should introduces another variable, clay temperature T_c, as defined in Eqs. (14)–(15). Analogous to granular temperature, the concept of "clay temperature" is introduced here as a state variable that represents the average kinetic energy associated with meso-scale structural energy fluctuations of clays. This concept is fundamentally linked to the structures and conditions of both clays and sands (see Appendix A). Notably, the proposed "clay temperature" corresponds directly to the meso-structural temperature of clays established by Wiebicke and Einav (2024).

$$p_v = g(T_c) \tag{14}$$

$$\eta_v = f(T_c) \tag{15}$$

ii) Clay temperature.

To close the above equation system, a constitutive formulation for the clay temperature must be introduced, a challenge in the existing literature. In the original kinetic theory, the concept of granular temperature is well-established by a balance equation derived from fluctuating kinetic energy. However, this study refrains from constructing a complete thermodynamic framework for two primary reasons: (i) applying this theory to clay yields incorrect viscosity predictions, as demonstrated in Fig. 7; and (ii) the calculation of granular temperature evolution necessitates numerous complex auxiliary equations, more than 10 in standard formulations (see Redaelli et al., 2016). Consequently, we introduce a "clay temperature" to directly replace the "granular temperature", thereby establishing a robust phenomenological model. This approach maintains physical interpretability while significantly enhancing computational efficiency, making it better suited for practical engineering applications.

We begin by considering the simple shear condition. Based on Eq. (10), which indicates that the granular temperature scales with the square of the shear rate and the particle diameter, a polynomial function of the shear rate is adopted to represent this relationship.

$$T_c = m_c d^n \dot{\gamma}^n \tag{16}$$

where m_c and n are viscous coefficients to describe the clay temperature.

Analogous to Eq. (11), the shear viscosity of clay is proposed:

$$\eta_c = \rho d T_c = m_c \rho d^{n+1} \dot{\gamma}^n \tag{17}$$

Analogous to Eq. (12), the viscous shear stress of clay is proposed:

$$\tau_v = \eta_c \dot{\gamma} = m_c \rho d^{n+1} \dot{\gamma}^{n+1} \tag{18}$$

Compared to the equations in Appendix C, the shear rate $\dot{\gamma}$ is not neglected but is implicitly incorporated through the evolution of the parameter T_c. Although the solid concentration ϕ is not explicitly included in the equations, its influence on the viscous stress is captured via the parameter m_c. A more precise quantitative relationship between ϕ and m_c can be established in the future using available experimental data.

iii) Clay's viscous mean stress.

To close the above equation system, a constitutive relation for the clay's viscous mean stress also must be introduced. Both the kinetic theory and experimental observations in granular flows suggest a constant ratio between viscous hydrostatic and shear stress during the fluid-like state (see Fig.2 (b) and Feng and Yin, 2025). By analogy, we extend this principle to clay, defining the viscous mean stress as:

$$\sigma_{n,v} = \frac{\tau_v}{\mu_v} \tag{19}$$

where μ_v is the viscous friction coefficient of the fluid-like state.

In summary, the viscous stress under simple shear test can be expressed as follows:

$$\boldsymbol{\sigma}_{2D,v} = \begin{bmatrix} \sigma_{n,v} \\ \tau_v \end{bmatrix} = \begin{bmatrix} m_c \rho d^{n+1} \dot{\gamma}^{n+1} / \mu_v \\ m_c \rho d^{n+1} \dot{\gamma}^{n+1} \end{bmatrix} \tag{20}$$

where $\boldsymbol{\sigma}_{2D,v}$ is the simplified viscous stress vector under simple shear test; $\sigma_{n,v}$ and τ_v are the viscous vertical stress, viscous shear stress under simple shear test, respectively.

Based the stress at the simple shear condition, the 3D stress tensor can be developed using the clay viscosity and viscous mean stress, which is given as follows:

$$\eta_c = \rho d T_c = m_c \rho d^{n+1} |\dot{\boldsymbol{\gamma}}|^n \tag{21}$$

$$p_v = m_c \rho d^{n+1} |\dot{\gamma}|^{n+1} \Big/ \mu_v \tag{22}$$

where $|\dot{\gamma}|$ is the equivalent shear rate, i.e., the second invariant of the deviatoric strain rate tensor, calculated via $|\dot{\gamma}| = \sqrt{\dot{\gamma} : \dot{\gamma}}$.

Remark 2. As discussed above, the proposed hydrodynamics-based model is based on the incompressibility assumption for clay's fluid-like state, similar to the widely-used $\mu(I)$ rheology (GDR-MiDi, 2004; Jop et al., 2006; Forterre and Pouliquen, 2008). Future work may consider a modified hydrodynamics-based model that incorporates rate-induced dilatancy for clay to give a broader application.

3.4. CSHM formulation

Following the framework discussed, the CSHM is formulated through the combination of quasi-static and viscous contributions. In this model, the rate-independent critical-state-based model is used for modeling quasi-static stress, while the proposed rate-dependent hydrodynamic model addresses the viscous stress. During the transition from solid-like to fluid-like states, the primary stress governing clay behavior shifts from quasi-static to viscous. This model replicates solid-like behaviors, including nonlinear elasticity, stress dilatancy, and critical state, while also simulating non-Newtonian fluid-like characteristics.

In summary, the unified effective stress is expressed as follows:

$$\boldsymbol{\sigma}_s^{t+1} = \boldsymbol{\sigma}_{qs}^{t+1} + \boldsymbol{\sigma}_v^{t+1} = \boldsymbol{\sigma}_{qs}^{t} + d\boldsymbol{\sigma}_{qs}^{t} + \boldsymbol{\sigma}_v^{t} + d\boldsymbol{\sigma}_v^{t} \tag{23}$$

where $\boldsymbol{\sigma}_{qs}^{t+1}$ and $\boldsymbol{\sigma}_v^{t+1}$ are quasi-static and viscous stress at the $t+1$ step, respectively; $\boldsymbol{\sigma}_{qs}^{t}$ and $\boldsymbol{\sigma}_v^{t}$ are quasi-static and viscous stress at the t step, respectively; $d\boldsymbol{\sigma}_{qs}^{t}$ and $d\boldsymbol{\sigma}_v^{t}$ are quasi-static and viscous stress increments at the t step, respectively.

The quasi-static stress increment tensor $d\boldsymbol{\sigma}_{qs}^{t}$ is expressed as follows:

$$d\boldsymbol{\sigma}_{qs}^{t} = \mathbf{D}_{qs}^{e} : (d\boldsymbol{\varepsilon} - d\boldsymbol{\varepsilon}^{p}) = \mathbf{D}_{qs}^{ep} : d\boldsymbol{\varepsilon} \tag{24}$$

where $\mathbf{D}_{qs}^{ep}$ is the fourth-order tensor of the elastoplastic modulus, expressed as follows:

$$\mathbf{D}_{qs}^{ep} = \mathbf{D}_{qs}^{e} - \frac{\mathbf{D}_{qs}^{e} \frac{\delta g}{\delta \sigma_{qs}} \left(\frac{\partial f}{\partial \sigma_{qs}}\right)^{T} \mathbf{D}_{qs}^{e}}{\left(\frac{\partial f}{\partial \sigma_{qs}}\right)^{T} \mathbf{D}^{e} \frac{\partial g}{\partial \sigma_{qs}}} \tag{25}$$

where $\mathbf{D}_{qs}^{e}$ denotes the fourth-order elastic stiffness tensor, f and g are the yield function and flow rule, respectively.

The incremental viscous stress tensor $d\boldsymbol{\sigma}_v^{t}$ is expressed as follows:

$$d\boldsymbol{\sigma}_v^{t} = \frac{m_c \rho d^{n+1}}{\mu_v} \left(\left| \frac{d\gamma}{dt} \right|^{n+1} - |\dot{\gamma}^{t}|^{n+1} \right) \mathbf{I} - 2 m_c \rho d^{n+1} |\dot{\gamma}^{t}|^{n+1} \left(\frac{d\boldsymbol{\varepsilon}}{dt} - \dot{\boldsymbol{\varepsilon}}^{t} \right) \tag{26}$$

where $d\boldsymbol{\varepsilon}$ and $d\gamma$ are the strain and deviatoric strain increments, respectively; $|\square|$ denotes the norm; $\dot{\boldsymbol{\varepsilon}}^{t}$ and $\dot{\gamma}^{t}$ are the strain rate tensor and deviatoric strain rate tensor at the t step, respectively, expressed as follow:

$$\dot{\boldsymbol{\varepsilon}} = \frac{1}{2} \left((\nabla \cdot \boldsymbol{u}) + (\nabla \cdot \boldsymbol{u})^{T} \right) \tag{27}$$

$$\dot{\gamma} = \dot{\boldsymbol{\varepsilon}} - tr(\dot{\boldsymbol{\varepsilon}}) \mathbf{I} \tag{28}$$

4. Model parameters and implementation

Table 1 lists the eight parameters of the proposed critical-state-based hydrodynamic model, which will be divided into two groups:

(i) The first group is related to the parameters of the critical-state-based model: Poisson's ratio ν and swelling index κ describe the elastic behavior; the slope of critical state line M_c and compression index λ describe the plastic behaviors. All seven parameters can be determined by a standard calibration process from triaxial and oedometer tests.

(ii) The second group is related to the parameters of the hydrodynamic-based rheology model: ρ is the dry density, representing the density of solid skeleton; d is the representative diameter, which can take the value of 1 m. The viscous coefficients m_c and n can be obtained from the rheometer test. The viscous friction coefficient μ_v should be determined via the rheometer test results. The viscous coefficients m_c and n in this new hydrodynamic-based model basically govern the viscous property of the clay, and will be detailly discussed in Section 5.

In this study, the undrained simple shear test is utilized for the implementation of the CSHM. It is selected because it is the only available element test for clay that can capture large deformation characteristics and exhibit both solid-like and fluid-like behaviors concurrently, as discussed in Section 2. To achieve such a purpose, a forward Eulerian explicit integration algorithm is employed to obtain the effective stress (see Eq. (29)). A small time step $dt = 10^{-4}$ s is employed to guarantee the numerical convergence.

$$\boldsymbol{\sigma}_{2D,qs}^{t+1} = \boldsymbol{\sigma}_{2D,qs}^{t+1} + \boldsymbol{\sigma}_{2D,v}^{t+1} = \boldsymbol{\sigma}_{2D,qs}^{t} + d\boldsymbol{\sigma}_{2D,qs}^{t} + \boldsymbol{\sigma}_{2D,v}^{t} + d\boldsymbol{\sigma}_{2D,v}^{t} \tag{29}$$

where $d\boldsymbol{\sigma}_{2D,qs}^{t}$ and $d\boldsymbol{\sigma}_{2D,v}^{t}$ are the quasi-static stress increment tensor and quasi-static stress increment tensor, can be obtained from Eqs. (24)–(26).

Remark 3. A dimensional analysis of the parameters is as follows: the viscous coefficient n and viscous friction coefficient μ_v are unitless. The viscous consistency coefficient m_c, however, is a dimensional parameter whose units must balance the entire stress equation. The fundamental dimensions of m_c are $L^{(1-n)}T^{(n-1)}$. In SI units, this is equivalent to $(m/s)^{(1-n)}$, which represents the velocity-dependent part of this unit. This indicates that the numerical value of m_c is effectively normalized by a characteristic velocity, $(1\ m/s)^{(1-n)}$.

5. Model evaluation

A series of element simulations, employing a constant-volume simple shear test under the forward Euler explicit integration scheme, is conducted to evaluate the performance of the proposed Critical-State-based Hydrodynamic Model (CSHM). The evaluation systematically assesses the CSHM across three distinct regimes: (i) a pure quasi-static stress component at the small strain rate regime, (ii) a pure viscous stress component at the large strain rate regime (iii) the unified CSHM framework at the whole strain rate regime (see Table 2). Specifically, the influence of the initial vertical stress is examined for the quasi-static stress component, while viscous coefficients (m_c and n) are analyzed for the viscous stress component. The CSHM analysis incorporated all

Table 2
Summary of element simulation examples with specific purposes in this study.

Aspects	Specific evaluation purpose	Influencing factors	Reference
Quasi-static stress	Performance at the solid-like state	Initial vertical stress	Section 5.1
Viscous stress	Performance at the fluid-like state	Viscous coefficients n and m_c	Section 5.2
CSHM	Ability to describe the solid-to-fluid phase transition	Initial vertical stress, viscous coefficients n and m_c	Section 5.3

influencing factors.

5.1. Simulation using pure quasi-static stress part

This subsection first investigates the quasi-static solid-like stress model's performance at the solid-like state. In order to integrate the quasi-static stress, a forward Eulerian explicit integration procedure with a small time step of $dt = 10^{-4}$ s is used. Given the solid-like stress model's strain rate-independence, only the shear strain, 0.20, is given. Table. 1 gives the parameters required. Different initial vertical stress $\sigma_{n,0}$ = 100, 500, and 1000 kPa are considered. During this study, $\sigma_{n,qs}$ and τ_{qs} are employed to describe the effective vertical stress and shear stress in the undrained simple shear test, respectively.

Fig. 8 shows the simulation results of solid-like stress using constant-volume simple shear tests with varying initial vertical stresses. As shown in Fig. 8(a), all specimens converge toward the critical-state line, with higher initial vertical stresses correlating to greater residual shear stresses. Fig. 8(b) highlights shear-induced contractive behavior under undrained conditions, where mean vertical stress progressively increases until stabilizing at the critical-state residual stress. These simulations focus on the normally consolidated (NC) clay, as the rheometer tests, only capable of phase transition analysis, are conducted under NC conditions. Over-consolidated (OC) clays, which display shear-induced dilation, are ignored due to the absence of OC experimental data.

These results show that the clay's quasi-static stress stabilizes at the critical value at the small strain around 0.05 and remains invariant with further strain accumulation. These observations align with a critical-state elastoplastic model for granular phase transitions, as observed in the previous study (Feng et al., 2025), suggesting the solid-like stress model is effective to capture the clay's phase transition.

5.2. Simulation using pure viscous stress part

This subsection evaluates the phenomenological hydrodynamics-based model through constant-volume simple shear test simulations. Key input parameters are provided in Table 1, where different values of the viscous coefficient $n = -0.3$, 0.0, and 0.3 are considered. The viscous coefficient m_c considers different values of 0.005, 0.025, and 0.100. Dry density ρ takes a value of 1000 kg/m^3. Representative diameter d takes the value of 1 m.

Fig. 9 illustrates the simulation results using the phenomenological hydrodynamics-based rheology model with different values of viscous parameter n. As is shown the Fig. 9(a) and 9(b), at lower shear rates, the system exhibits negligible viscous stress, consistent with a solid-like dominated behavior. As the shear rate increases, the viscous stress rises, marking a transition to a fluid-like regime where rate-dependent viscous flow becomes dominant. This transition from a solid-like to a fluid-like state highlights the dominance of viscous stress, demonstrating that the proposed hydrodynamics-based model effectively captures the fluid-like behavior of clay. Additionally, Fig. 9(a) shows that the viscous coefficient n significantly influences the magnitude of the viscous stress. Specifically, an increase in n leads to a corresponding rise in viscous stress. This highlights the critical role of the viscous coefficient n in modulating the stress response within the hydrodynamics-based model. Fig. 9(b) further illustrates the evolution of viscosity under varying viscous coefficients n. A negative n results in a gradual decrease in viscosity, indicating shear-cooling (thinning) behavior. Conversely, a positive n leads to an increase in viscosity, characteristic of shear-heating (thickening) behavior. Notably, when n is zero, the viscosity remains constant. This symmetry in the proposed hydrodynamics-based rheology model effectively captures the diverse rheological responses based on the sign and magnitude of n.

We further obtain the evolution of clay temperature T_c under varying viscous coefficients n (see Fig.10(a)). The symmetry in the clay temperature-shear rate curves arises from the viscous coefficient n: positive n induces the activation of clay temperature (heating), promoting shear-thickening behavior, whereas negative n suppresses the activation of clay temperature (cooling), consistent with shear-thinning. When $n = 0$, T_c remains constant, indicating no soil temperature coupling to shear rate. Furthermore, Fig.10(a) reveals the physical meaning of coefficients m_c and n. Coefficient $m_c d$ physically represents the referenced clay temperature at the shear rate $\dot{\gamma}$ of 1 s^{-1}, while n governs the slope of the clay temperature-shear rate relationship. These interpretations can also be derived from the Eq.(16).

Extensive experiment indicates the clay exhibits shear-thinning behavior (e.g., Yi et al., 2018; Liu et al., 2023; Wei et al., 2025), indicating that a negative n is required in the proposed hydrodynamics-based model for clay. With an interesting comparison between the clay and granular temperature, we obtain the evolution of granular temperature based on our prior study (Feng et al., 2025), shown in Fig. 10(b). It shows that granular media undergo continuous heating under shear, leading to shear-thickening behavior. This aligns with Bagnoldian rheology (Bagnold, 1954), where viscous stress scales quadratically with shear rate ($\tau_v \propto \dot{\gamma}^2$), and viscosity increases linearly with shear rate ($\eta_v = \tau_v/\dot{\gamma} \propto \dot{\gamma}$) (Fall et al., 2010). In contrast, clay's viscous response is shear-thinning (i.e., cooling). This divergence underscores that the phase transition in sand is a shear-heating process, adequately described by existing kinetic theory, and viscous stress models developed for granular media are inadequate for capturing clay's viscous stress. Note that future work can establish a relation of granular and clay temperatures, using reliable experimental data.

We further evaluate the phenomenological hydrodynamics-based model with different viscous coefficient m_c of 0.005, 0.025, and 0.100. The viscous coefficient n is set as -0.3. Dry density ρ takes a value of 1000 kg/m^3. Representative diameter d takes the value of 1 m.

Fig. 11 illustrates the simulation results with different viscous

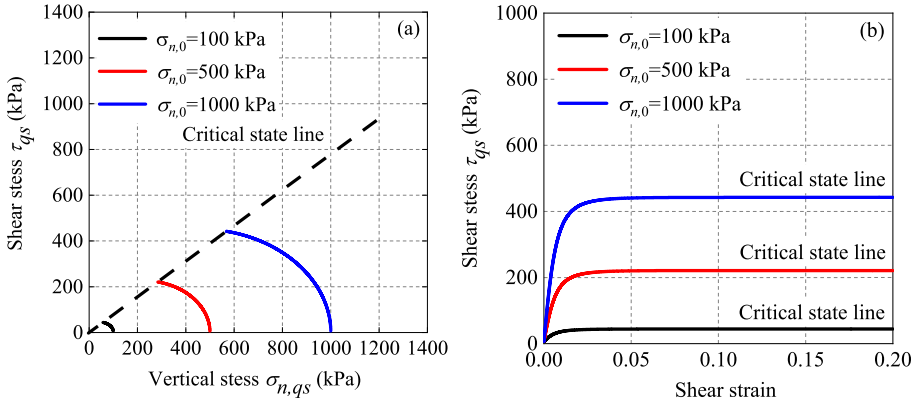

Fig. 8. Simulation of solid-like stress with various initial vertical stresses. (a) The vertical and shear stresses. (b) The shear strain and shear stress.

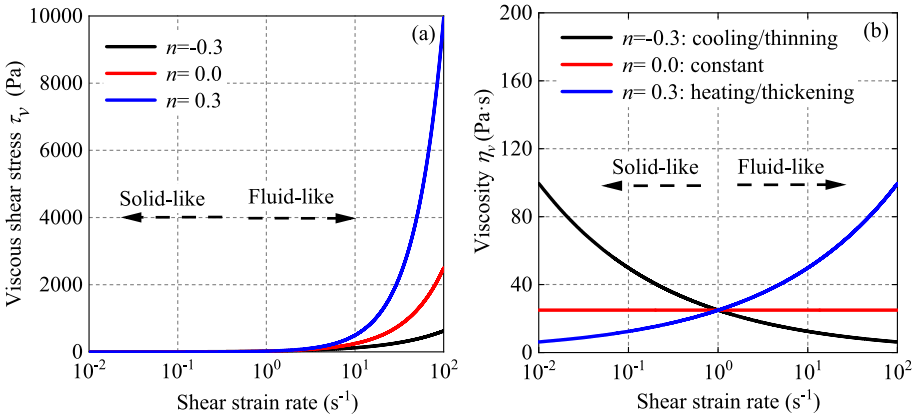

Fig. 9. Simulation results of the hydrodynamics-based fluid-like stress model with different values of the viscous coefficient *n*. (a) Development of viscous shear stress; (b) Development of viscosity.

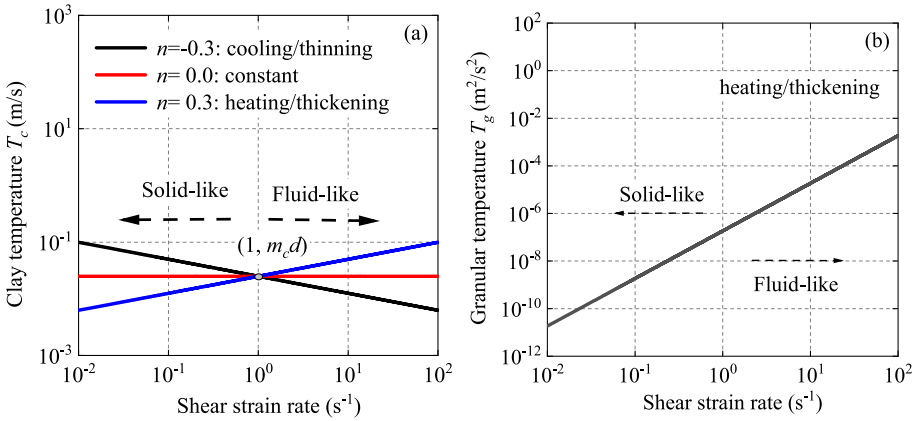

Fig. 10. Comparison between clay temperature and granular temperature. (a) Development of clay temperature; (b) Development of granular temperature (parameter from Feng et al., 2025).

coefficient m_c. In Fig. 11(a), the viscous stress is negligible at shear rates below approximately 10^{-1} s^{-1}, indicating a solid-like regime. Beyond this threshold, the viscous stress increases significantly, indicating the clay system gradually transitions into a fluid-like state. Fig. 11 (b) demonstrates that smaller viscous parameter m_c can generate smaller viscosity. Furthermore, Fig. 11(c) reveals the mathematical interpretation of m_c: it corresponds to the value of the clay temperature at a reference shear rate of 1 s^{-1} and reference diameter of 1 m in logarithmic coordinates.

5.3. Simulation using CSHM

Constant-volume simple shear test simulations using CSHM are performed in this section. The input parameters for the model are summarized in Table. 1, where different values of initial mean stress (i.e., $\sigma_{n,0}$ = 100, 300, and 500 Pa) and different values of the viscous parameters (i.e., n = 0.3, 0.0, and − 0.3; m_c = 0.005, 0.025, and 0.100) are considered. A small time step ($dt = 10^{-4}$ s) is used to ensure numerical stability, with total simulation durations of 100 s.

5.3.1. Phase transition mechanism

This subsection first evaluates the efficiency of CSHM in capturing the phase transition of clay. Specifically, we compare the quasi-static stress part, the viscous stress part, and the total stress using CSHM. An initial mean stress $\sigma_{n,0}$ = 500 Pa is considered. To characterize the shear-thinning behavior of clay, a negative viscous parameter n = −0.3 is employed. The viscous parameter m_c = 0.025 is considered. The strain rate path follows a similar approach to that in Feng et al. (2025). At the beginning, a shear rate of 10 s^{-1} and zero strain acceleration are given in 5 s, then a strain rate acceleration of 100 s^{-2} is applied from 5 s to 20 s.

Figs. 12 and 13 compare the simulation results for vertical stress and shear stress, respectively. The total stress predicted by the CSHM is represented by a black line, the quasi-static stress component by a red line, and the viscous stress component by a blue line. The total stress undergoes a dynamic evolution. Specifically, the vertical stress initially decreases, then increases slowly, and finally undergoes a rapid increase (Fig. 12). Similarly, the shear stress first increases rapidly, then at a slower rate, and finally accelerates again. This complex evolution is primarily attributed to the dynamic evolution of the clay's quasi-static and viscous stress components: at low shear rates (e.g., shear rate from 0 to 10^{-1} s^{-1}), quasi-static stress governs, reflecting solid-like behavior. At high shear rates (shear rate higher than 10^2 s^{-1}), viscous stress dominates, indicating fluid-like states. This confirms the model's effectiveness in capturing both solid and fluid response during the clay flows. These observations are also revealed by exiting sand's phase transition model (refer to Feng and Yin, 2025).

To quantitatively describe the phase transition of clay, distinguishing between its solid-like and fluid-like behaviors, two distinct transitional points are defined based on the proposed CSHM (see Figs. 12 and 13):

Transitional point A is defined as the critical state point, which occurs when the quasi-static stress component attains its critical value. Reaching this point signifies that the clay has entered the critical state, transitioning from solid-like behavior to a state of continuous deformation under constant stress and volume. This transition is

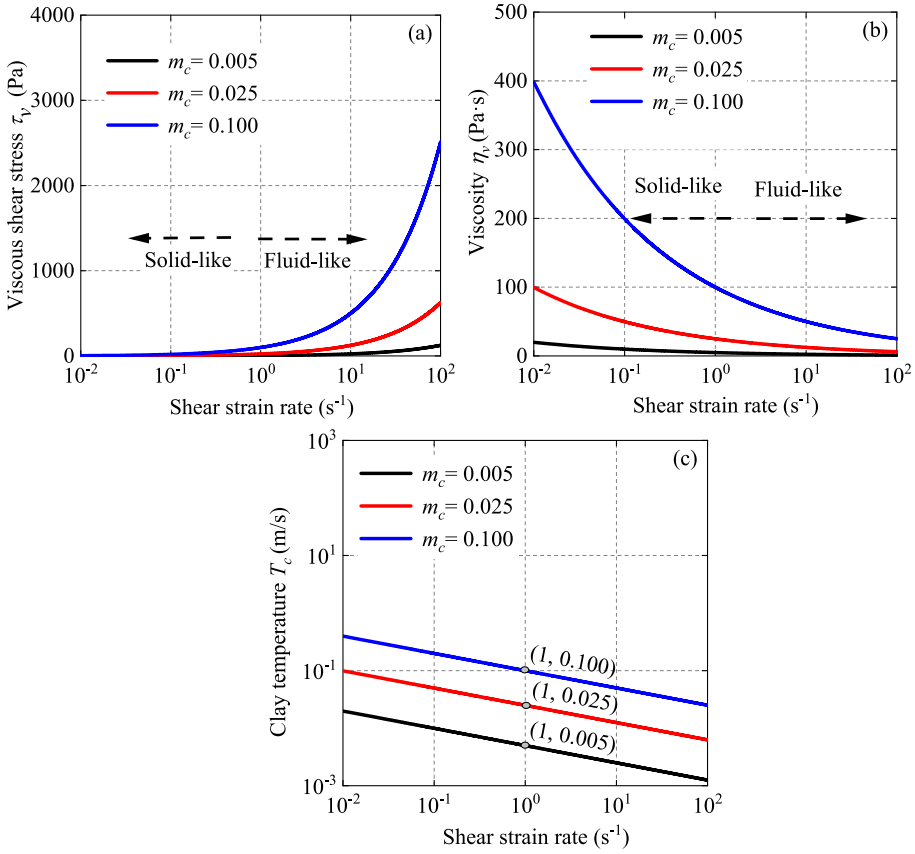

Fig. 11. Simulation results of the hydrodynamics-based fluid-like stress model with different values of the viscous coefficient m_c. (a) Development of viscous shear stress; (b) Development of viscosity; (c) Development of clay temperature.

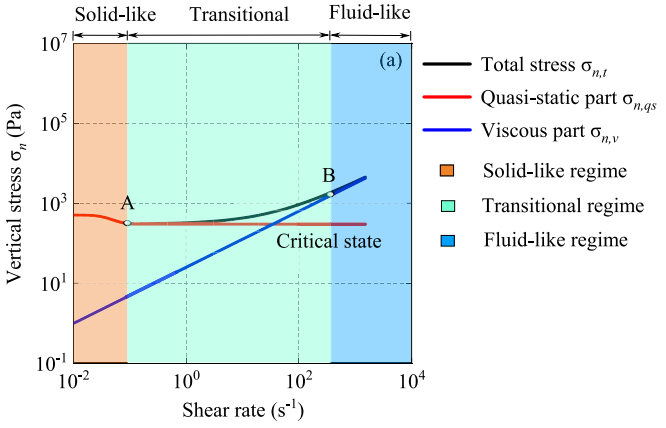

Fig. 12. Comparison of the vertical stress from the quasi-static stress part, viscous stress part, and total stress CSHM.

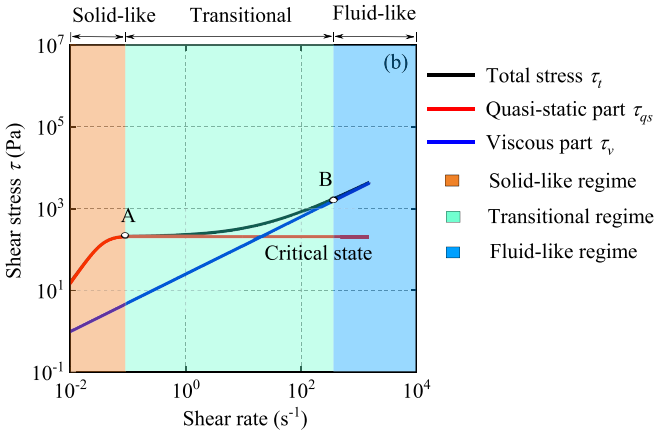

Fig. 13. Comparison of the shear stress from the quasi-static stress part, viscous stress part, and total stress CSHM.

fundamentally governed by the critical state theory embedded within the quasi-static component of the CSHM.

Transitional point B is defined as the point where the contribution of quasi-static stress to the total stress becomes negligible (i.e., $\frac{|\sigma_{qs}|}{|\sigma_{qs}|+|\sigma_v|} \approx 0$), indicating the dominance of the viscous stress component. At this point, the clay transitions from a transitional state to a fluid-like state, a regime now governed almost entirely by the viscous stress. This transition is basically controlled by the state variable, clay temperature, as defined within the viscous stress component of the CSHM.

Based on the above two transitional points, three different regimes can be divided (see Figs. 12 and 13):

(i) **Solid-like regime at the small strain rate range** (i.e., from the the initial state to point A): Within this regime, the total stress is predominantly governed by the quasi-static component, while the viscous stress contribution is negligible, i.e., satisfying the condition $\frac{|\sigma_v|}{|\sigma_{qs}|+|\sigma_v|} \approx 0$. Note that the quasi-static stress component in the proposed CSHM is intrinsically rate-independent, the apparent rate-dependent behavior observed in Figs. 12 and 13 arises from strain-hardening. Specifically, a higher applied strain rate induces the accumulation of strain, which consequently elevates the rate-independent quasi-static stress.

(ii) **Transitional regime at the large strain rate range** (i.e., from point A to point B): Within this regime, the clay's mechanical response is governed by a combination of quasi-static and viscous stresses. The quasi-static stress component maintains the residual strength characteristic of the critical state, whereas the viscous stress component increases with the applied strain rate via the clay temperature.

(iii) **Fluid-like regime at very large strain rate regime** (i.e., state after point B):Within this regime, the clay's behavior is predominantly governed by viscous stress, while the contribution of quasi-static stress becomes negligible. This signifies that the material has fully transitioned into a fluid-like state.

Remark 4. Note that the proposed model describes a transition from a solid-like to a fluid-like state, rather than a transition between a purely solid and a purely fluid phase. In our formulation, the vertical (confining) pressure remains finite throughout the solid-like to fluid-like transition. By contrast, a pure solid-fluid transition would require the pressure to vanish, corresponding to an unjamming transition. Our model can, in principle, represent this unjamming behavior: as the confining pressure decreases, the solid-like elastoplastic pressure tends to zero. In this limit, the solid-like shear stress also degrades to zero. The material response is governed solely by the non-Newtonian fluid-like relation in our model, corresponding to a fully unjammed regime.

5.3.2. *Influencing factors analysis*

In this study, we further examine the influence of initial vertical stress on the clay flow behavior. An initial mean stress $\sigma_{n,0} = 100$, 300, 500 Pa is considered. To characterize the shear-thinning behavior of clay, a negative viscous parameter $n = -0.3$ is employed. The viscous parameter $m_c = 0.025$ is considered.

Fig. 14 shows the variations in vertical and shear stress under different initial vertical stresses. The findings reveal that initial vertical stress has a pronounced impact on clay flow, especially at low strain rates. Conversely, at elevated strain rates, both vertical and shear stresses tend to converge regardless of the initial vertical stress. This indicates that the initial condition of the clay exerts little influence in the high strain rate regime. These observations are consistent with the phase transition model for sand proposed by Feng et al. (2025), demonstrating the validity of the critical-state-based hydrodynamic model.

This study further evaluates the proposed CSHM's ability to replicate strain rate-dependent rheological behaviors, including shear-thinning and shear-thickening responses. Simulations were conducted with viscous parameter n set to 0.3, 0.0, and − 0.3. An initial mean stress $\sigma_{n,0} = 500$ Pa is considered. The viscous parameter $m_c = 0.025$ is considered.

As illustrated in Fig. 15, higher values of the viscous parameter n result in increased viscous stresses; however, they do not affect the solid-like responses, which are governed by the critical-state-based elastoplastic model. This finding confirms that the proposed model can not only describe the phase transition of clay but also apply to other material with different rheological behaviors, governed by parameter n.

We further evaluate the proposed CSHM by considering different viscous coefficicent m_c. Simulations were conducted with viscous parameter m_c set to 0.005, 0.025, and 0.100. An initial mean stress $\sigma_{n,0} = 500$ Pa is considered. The viscous parameter $n = -0.3$ is considered.

As illustrated in Fig. 16, higher values of m_c result in significantly increased viscous stresses at high strain rates. Conversely, the solid-like response at low strain rates remains unaffected, as it is governed solely by the critical-state-based quasi-static component of the model. This finding confirms that the viscous parameter m_c predominantly influences the clay's fluid-like behavior, while the solid-like response is controlled independently by the critical state mechanics.

6. Experimental validation

A series of element tests are simulated to validate the effectiveness of the proposed CSHM in capturing the solid-fluid phase transition of clay. The validation addresses three key aspects: the pure quasi-static stress component, the pure viscous stress component, and the integrated CSHM (see Table 3). Since the reliability of the quasi-static stress component has been extensively established in prior literature (Schofield and Wroth, 1968; Yin et al., 2020), its validation is not repeated here. Instead, this study focuses on validating the proposed pure viscous stress component and the unified CSHM. Table 3 summarizes all test cases and their corresponding validation objectives. All simulations employed a constant-volume simple shear test under a forward Euler explicit integration scheme, as discussed in previous sections.

6.1. *Montmorillonite clay*

Wei et al. (2025) conducted the rheometer test to investigate the viscous characteristics of montmorillonite clay with different water content at $W_L = 252\%$, 216%, 180%, and 144%. Due to unreported solid-state parameters (i.e., critical-state-based parameters), validation focuses on the prposed hydrodynamics-based viscous stress model. Dry density ρ takes a value of 2000 kg/m^3. Representative diameter d takes the value of 1 m. Different values of parameter $m_c = 0.004$, 0.0065, and 0.007 are considered, with the viscous parameter n setting as −0.5 (see Table. 1).

Using the integration algorithm described in Section 4, viscosity-strain rate curves and viscous shear stress-shear rate curves are obtained, as shown in Fig. 17. The figure also includes corresponding experimental measurements from the rheometer tests. The agreement

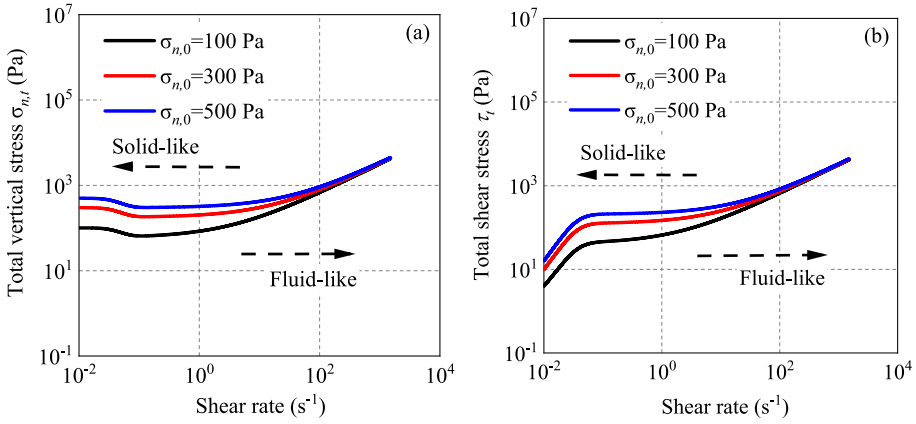

Fig. 14. Simulation results of the critical-state-based hydrodynamic model under various initial vertical stresses. (a) The total vertical stress; (b) The toal shear stress.

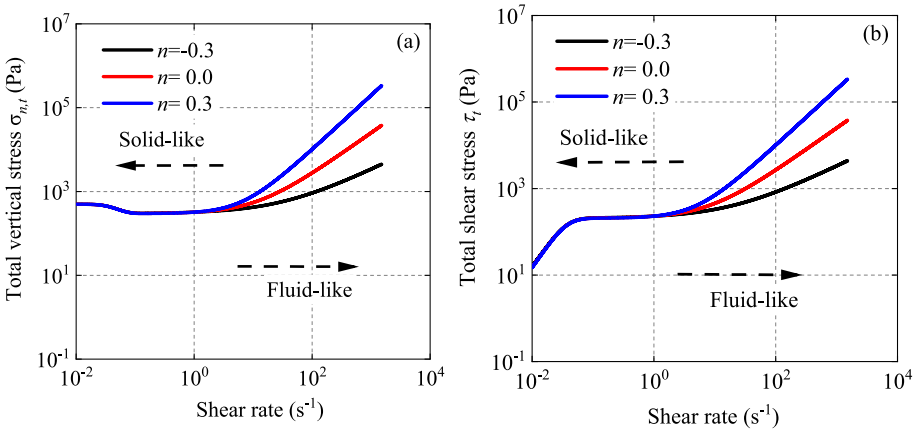

Fig. 15. Simulation results of the critical-state-based hydrodynamic model with different values of the viscous parameter *n*. (a) The total vertical stress; (b) The total shear stress.

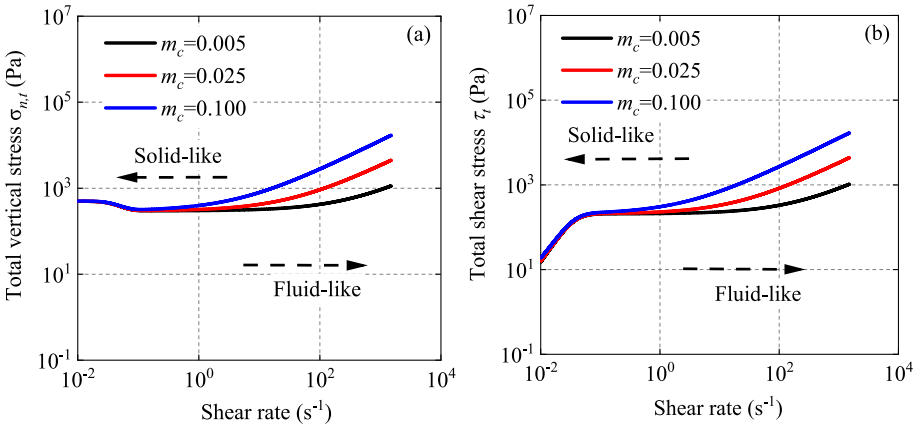

Fig. 16. Simulation results of the critical-state-based hydrodynamic model with different values of the viscous parameter m_c. (a) The total vertical stress; (b) The total shear stress.

Table 3
Summary of validation examples with specific purposes in other studies or this study.

Validation purpose	Employed soils	Reference
Pure quasi-static stress model	–	Yin et al., 2020
Proposed viscous stress model	Montmorillonite clay	Section 6.1
Proposed CSHM	Malaysian kaolin clay	Section 6.2
Proposed CSHM	Natural kaolin clay	Section 6.3

between simulations and measurements underscores the ability of the proposed hydrodynamics-based viscous stress model to reasonably approximate experimental behavior. Furthermore, the comparison confirms the model's capacity to replicate shear-thinning behavior (with $n = -0.5$). Furthermore, the validation demonstrates two key trends: (i) the viscous exponent n remains invariant ($n = -0.5$) across water contents, and (ii) the viscous coefficient m_c decreases systematically with increasing water content.

6.2. Malaysian kaolin clay

To further validate the proposed CSHM for the phase transition of clay, we utilize experimental results from Malaysian kaolin clay as reported by Yi et al. (2018). A preliminary discussion of these results is provided in Section 2.2. Using the reported parameters for quasi-static stress, the CSHM is applied to simulate the total shear stress. Initially, viscous shear stress-shear rate curves are used to determine the viscous parameters m_c and n. Subsequently, these parameters, along with the critical-state-based parameters from Yi et al. (2018), are used in the simulation. These parameters are detailed in Table 1.

Fig. 18 presents the simulation results from the proposed CSHM alongside experimental data from Yi et al. (2018). This comparison underscores the model's ability to accurately approximate laboratory element tests, and demonstrates the effectiveness of the proposed CSHM in describing the phase transition of clay. The model effectively captures the stress evolution in clay as it transitions from a solid-like to a fluid-like state. During the transition, the total shear stress initially increases at low strain rates until reaching the critical state, as indicated by the flat curve in Fig. 18. It then continues to increase at high strain rates, reflecting a shift in dominant stress from quasi-static to viscous. This observation can be well explained by the phase transition mechanism detailed in Section 5.3. For brevity, a repeated discussion is omitted here.

In addition, Fig.18 also shows that varying the water content in our model simultaneously influences the solid-like elastoplastic response (via Eqs. (4)–(7)) and the fluid-like viscous response (via Eqs. (16)–(18)), such that lower water content leads to a higher total stress.

6.3. Natural kaolin clay

This section further validates the CSHM's effectivenes in capturing the clay's phase transition via the experimental data for natural kaolin from Wei et al. (2025) (details see Section 2.2). Although critical-state-related parameters are not reported in the original study, the kaolin

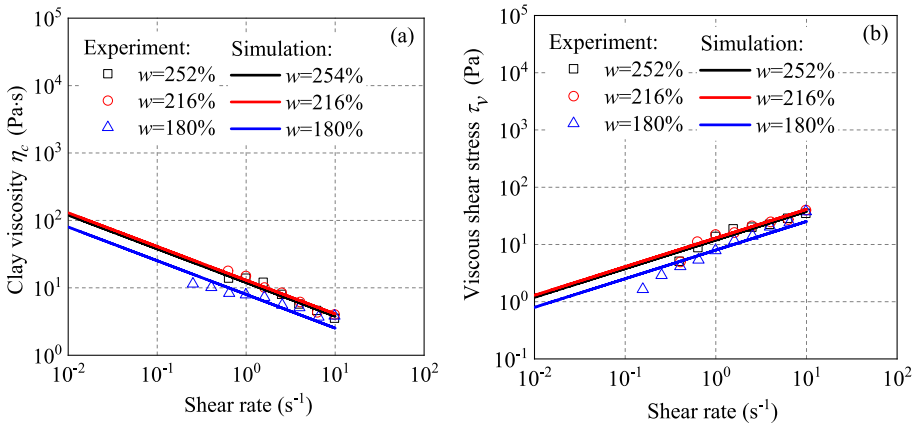

Fig. 17. Comparison between numerical and experimental results for montmorillonite clay. (a) Comparison of the viscosity; (b) Comparison of the viscous shear stress.

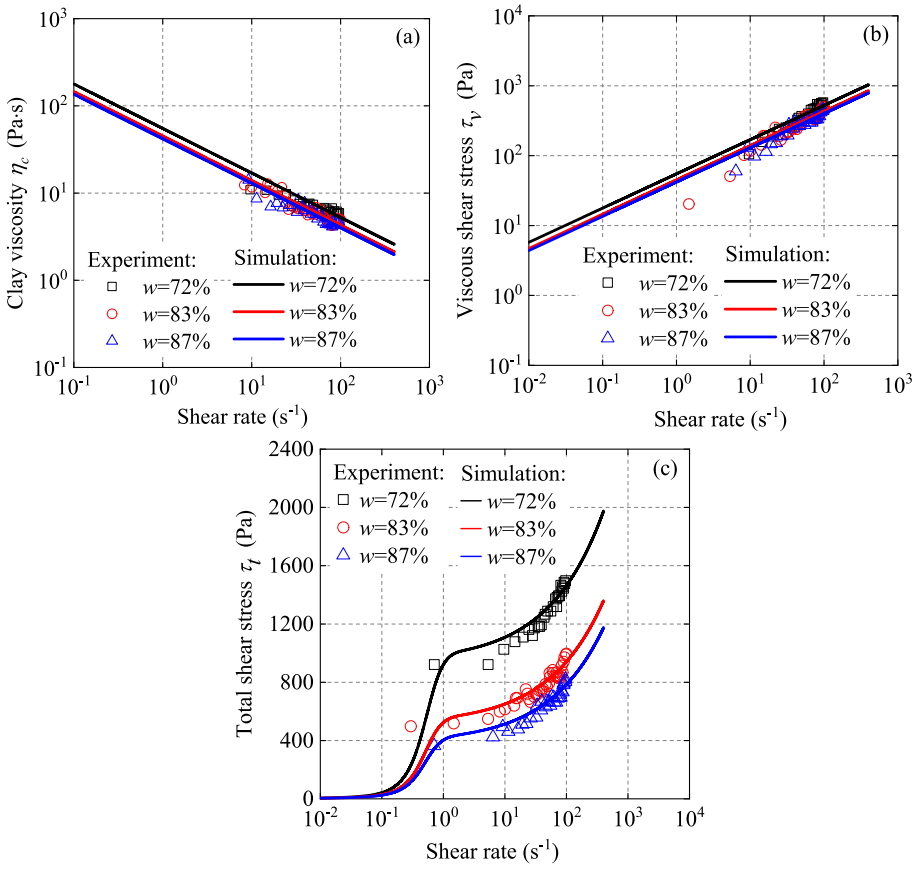

Fig. 18. Comparison between numerical and experimental results for Malaysian kaolin clay. (a) The viscosity; (b) The viscous shear stress; (c) The total shear stress.

clay's properties from Section 6.2 are adopted here as a representative analog. Accordingly, the quasi-static stress parameters from Section 6.2 are employed in this subsection. Viscous parameters are assigned as follows: $m_c = 0.003$, 0.325, and 0.044, corresponding to water contents of 59%, 49%, and 40%, respectively, while the exponent $n = -0.3$ is held constant across all samples.

Fig. 19 (a) and Fig. 19 (b) compares experimental viscosity-shear rate and viscous stress-shear rate curves for natural kaolin clay from rheometer tests with predictions from the proposed CSHM. The model closely approximates experimental results, particularly in the fluid-like regime where viscosity decreases linearly with shear rate (shear-thinning behavior), while viscous stress increases linearly with shear rate, consistent with the discussion in Section 5. This alignment confirms the model's efficacy for fluid-like states. Similar to the observation in Section 6.1, two key trends are also observed: (i) the viscous exponent n remains invariant ($n = -0.3$) across water contents, and (ii) the viscous coefficient m_c decreases systematically with increasing water content.

Fig. 19 (c) compares total shear stress predicted using the CSHM and experimental values. The numerical results from the CSHM closely match experimental data, demonstrating the CSHM's effectiveness in bridging solid and fluid states through the critical-state concept and clay temperature evolution.

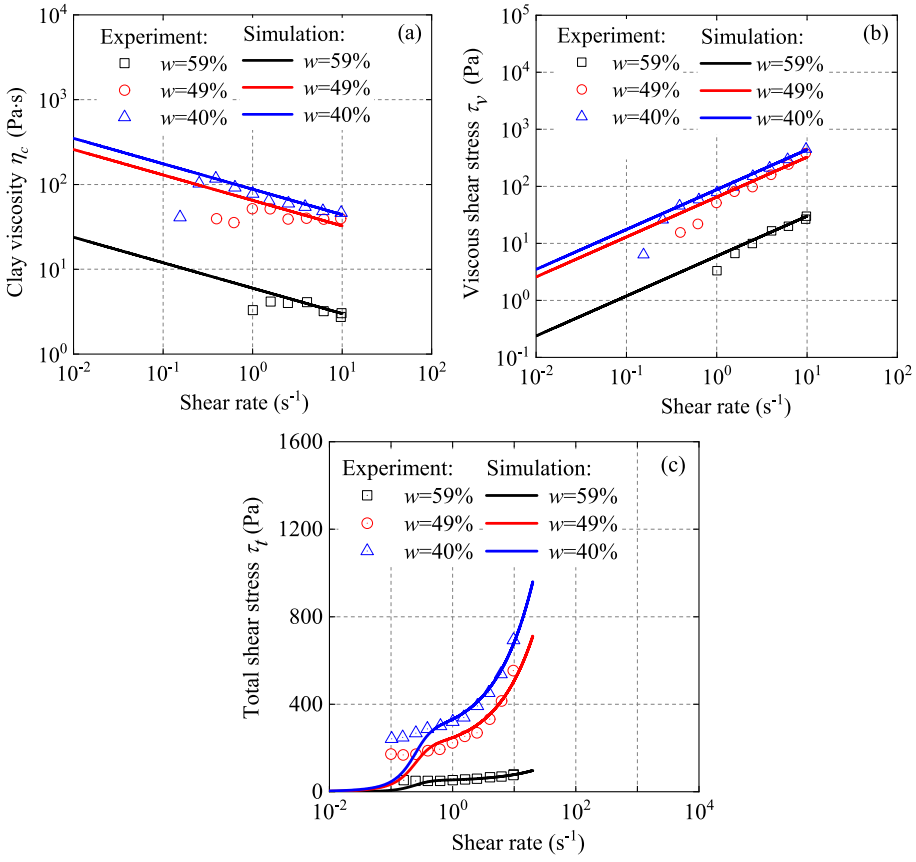

Fig. 19. Comparison between numerical and experimental results for natural kaolin clay. (a) The viscosity; (b) The viscous shear stress; (c) The total shear stress.

7. Discussion

7.1. Comparative discussion

To evaluate the performance of our CSHM relative to classic fluid-like viscous models, such as the Herschel-Bulkley (HB) and Bingham models, it is appropriate to compare the simulation results of the proposed CSHM with those of these established models. However, the Bingham model is a specific case of the more general HB model, corresponding to a flow index of $n_{HB} = 1$ in Eq. (30). Therefore, comparison with the general HB model alone is sufficient to demonstrate the effectiveness of our CSHM against a class of fluid-like viscous models.

$$\tau_t = \begin{cases} \tau_0 + m_{HB}|\dot{\gamma}|^{n_{HB}} & \text{if } |\tau_t| > \tau_0 \\ \dot{\gamma} = 0 & \text{otherwise} \end{cases} \tag{30}$$

where τ_0 is the yield stress, m_{HB} and n_{HB} are the viscous parameters of the HB model, corresponding to the viscous coefficients m_c and $n + 1$ in the hydrodynamic model.

We derive the relationship between total shear stress and shear rate from the HB model and compare it with the proposed CSHM. As shown in Fig. 20, the HB model and the proposed CSHM differ in the solid-like state but converge in the fluid-like state. The detailed discussion follows:

(i) In the solid-like state (the shear rate from 10^{-2} s^{-1} to 10^{0} s^{-1} in Fig. 20), the HB model treats clay as a rigid solid, maintaining constant stress at zero shear rates, which limits its ability to describe solid-like responses. Therefore, it cannot be considered a full-range solid-fluid phase transition model but rather a fluid-like stress model, describing stress in the fluid-like state. In contrast, the proposed CSHM can be seen as a full-range phase transition model, effectively capturing evolution of stress from the initial to the critical state, and eventually the fluid-like state.

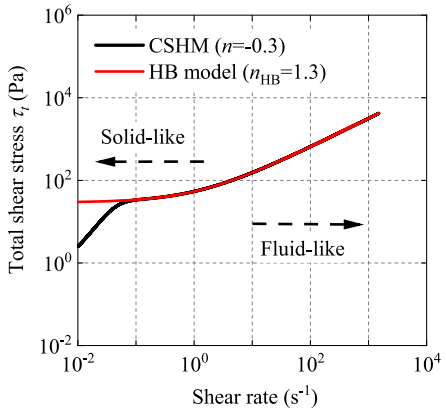

Fig. 20. Comparison of simulation results between proposed CSHM and HB model.

(ii) In the fluid-like state (the shear rate from 10^{0} s^{-1} to 10^{4} s^{-1} in Fig. 20), Both the HB model and the proposed CSHM account for complex rheological properties, including shear-thinning and shear-thickening behaviors. However, the proposed CSHM offers greater physical insight by incorporating the state variable "clay temperature", aligning with the phase transition framework used for sands. Additionally, it includes an evolution equation for viscous hydrostatic stress, a feature not present in the HB model.

(iii) Finally, it's worth noting that the HB model is a 2D stress model, whereas the proposed CSHM is a 3D stress model.

Furthermore, while techniques (e.g., Roy et al., 2017) exist to modify the HB model to describe the small strain-rate regime, these models still

fail to accurately capture the volumetric stress, a capability demonstrated by our CSHM.

7.2. Discussion of perspectives

Despite these advancements discussed, four points must be addressed to enhance the accuracy of the proposed CSHM in future research:

(i) **Consideration of time-dependent behaviors in the solid-like state.** The proposed CSHM employs the phase transition framework for sands, combining rate-independent elastoplastic stress (solid-like) with rate-dependent viscous stress (fluid-like), effectively capturing clay's phase transition. Unlike sands, clay in the solid-like state exhibits time-dependent behaviors, e.g., creep, stress relaxation, and strain-rate dependency at small strains, as described by Elastic Visco-Plastic (EVP) theory (Yin et al., 2020). These behaviors may differ from the time-dependent rheology of the fluid-like state at large strains. To reconcile these regimes, targeted experimental studies are needed to quantify the interplay between rate dependency in soil and fluid mechanics. Future work should aim to develop a unified description of time-dependent behavior across all states, potentially by integrating EVP principles into the proposed model.

(ii) **Consideration of complex time-independent behaviors in the solid-like state.** The proposed CSHM employs an elastoplastic MCC model for the solid-like stress, a simplified representation that does not capture advanced features such as principal stress rotation or fabric anisotropy. These factors may affect the stress path and yielding behavior in the solid-like regime, thereby influencing phase transition. Future work will incorporate anisotropic or rotational hardening laws into the elastoplastic component of the CSHM to enhance its general applicability.

(iii) **Consideration of over-consolidated clay.** The available experimental data used for validation derive from rheometer tests approximating simple shear of normally consolidated (NC, OCR = 1) clay. Hence, the current model is validated for NC conditions. However, the CSHM framework is formulated to allow the incorporation of OCR with a sub-loading or bounding surface approach in the MCC elastoplastic stress component. Note that the MCC model may be inaccurate for low stress levels due to curved NCL and CSL. Hence, extension of the model to over-consolidated clay with low stress levels will be pursued in future work with appropriate experimental data.

(iv) **Consideration of the hydrostatic stress in the fluid-like state.** To address the gap in defining viscous hydrostatic stress, this study proposes a formulation based on observations from granular flows, which suggests a constant viscous vertical-shear stress ratio (Feng et al., 2025). Despite this novel formulation, the evolution of hydrostatic stress remains undetermined under current experimental conditions, highlighting the need for further validation of this assumption through targeted studies.

Additionally, the focus of this study on the undrained condition stems from the high shear rate during the simple shear test (e.g., from 0 to $10^3\ s^{-1}$). At these rates, the loading time is substantially shorter than the characteristic time for pore-pressure dissipation in clay, justifying an undrained interpretation. Under the drained condition, where loading is sufficiently slow to allow complete pore-pressure diffusion, the viscous stress component of the model becomes negligible. The response in this regime is governed by the elastoplastic Modified Cam-Clay (MCC) model of the proposed framework, which is well-established for simulating drained clay behavior.

8. Conclusions

This study has proposed a novel critical-state hydrodynamic model (CSHM) that is both simple and robust, effectively capturing the nonlinear solid-to-fluid transition of clay. In specific, the model integrates quasi-static and viscous stresses to account for solid-like and fluid-like responses in clay, respectively. The quasi-static stress is modeled using a critical-state-based model, while the viscous stress is described through a new hydrodynamic model governed by the state variable "clay temperature". The model's performance has been initially assessed through simple shear test simulations and further validated against experimental data. The following key observations have been made:

(i) Simulations indicate that the critical-state-based quasi-static stress component effectively captures clay's solid-like responses. Meanwhile, the inferred hydrodynamics-based viscous stress component not only reproduces the shear-thinning behavior of clay in its fluid-like state but also captures shear-thickening responses in other materials, depending on the viscosity parameters within the model.

(ii) The numerical results from the CSHM closely match experimental data, demonstrating the CSHM's effectiveness in bridging solid-like and fluid-like states through the critical-state concept and clay temperature evolution.

(iii) Element simulation using the CSHM reveals the clay's phase transition: when the clay is in a solid-like state, the quasi-static stress is predominant, while the viscous stress plays a significant role for clay in a fluid-like state. This transition is characterized by two transitional points (i.e., critical-state point and viscous-stress-dominant point) and three different regimes (i.e., solid-like, transitional, and fluid-like).

(iv) While sand undergoes a shear-induced heating phase transition and is well described by the existing kinetic theory, clay exhibits shear-cooling, which our novel model accurately captures. The distinct viscous behavior between granular media and clay warrants further investigation.

(v) Unlike the traditional HB model, a 2D model describing stress in the fluid-like state, the CSHM is a 3D full-range phase transition model that captures evolution from initial to critical state, and eventually fluid-like state.

The developed CSHM effectively describes the intricate solid-to-fluid phase transition of clays across a wide strain rate range. This robust constitutive model provides a foundation for developing more accurate early numerical models and effective disaster assessment systems for geohazards, such as landslides and debris flows. Furthermore, these comprehensive findings significantly enhance the mechanistic understanding of large deformation dynamics in clay.

CRediT authorship contribution statement

Hang Feng: Writing – review & editing, Writing – original draft, Visualization, Validation, Methodology, Formal analysis, Conceptualization. **Zhen-Yu Yin:** Writing – review & editing, Supervision, Funding acquisition, Conceptualization. **Wei Cheng:** Writing – review & editing, Formal analysis, Conceptualization.

Declaration of competing interest

The authors declare that they have no known competing financial interests or personal relationships that could have appeared to influence the work reported in this paper.

Acknowledgements

This work was supported by the general research fund of the Research Grants Council (RGC) of the Hong Kong Special Administrative Region Government (HKSARG) of China (grant No. 15232224, T22-

607/24-N), and the Department of Science and Technology of Guangdong Province (Grant No.: K-ZGSZ).

Appendix A. Structure and deformation of sands and clays

This appendix describes the structures and deformation mechanisms of sands and clays:

(i) Structure: As shown in Fig. A1, the structure of sand is simple, comprising primarily discrete particles. In contrast, clay possesses a complex, multi-scale structure: its fundamental units are mineral sheets, which assemble into clay particles, and further into clay aggregates (Graham et al., 1983). Furthermore, the small size of these mineral sheets gives rise to significant electrochemical interactions, which dominate clay's mechanical behavior and distinguish it fundamentally from sand (Mitchell and Soga, 2005).

(a) Sand structure (b) Clay structure

Fig. A1. The structure in sand and clay: (b) Sand structure; (c) Clay structure.

(ii) Deformation mechanism: During loading, clay deformation is complex and involves: (a) The collapse, expansion, and rearrangement of large pores between clay aggregates; (b) The movement of clay particles; (c) The breakdown of clay aggregates into individual platelets, a process mechanically analogous to particle crushing in granular media (Wiebicke and Einav, 2024).

These structures and deformation mechanisms suggest that clay aggregates or particles undergo sliding and collisions, exhibiting energy dissipation pathways similar to sands, including frictional and collisional interactions (Jaeger et al., 1996). Consequently, total effective stress can be conceptualized as the sum of frictional and collisional components. In this context, "clay temperature" is proposed as a representation of the average kinetic energy of these meso-scale structural fluctuations.

Notably, the proposed "clay temperature" corresponds to the meso-structural temperature of clay introduced by Wiebicke and Einav (2024). Furthermore, the above deformation mechanism is supported by experimental observations of clay from Hicher et al. (2000), Cotecchia et al. (2019), and Guglielmi et al. (2024).

(a) Sand stress decomposition (b) Clay stress decomposition

Fig. A2. The stress mechanism in sand and clay: (b) Sand stress decomposition; (c) Clay stress decomposition.

(iii) **Granular temperature and clay temperature**: The concept of granular temperature originates from the kinetic theory (Jenkins and Savage, 1983; Garzó and Dufty, 1999): (a) it is calculated by a balance equation derived from fluctuating kinetic energy; (b) it possesses a clear physical interpretation as particle velocity fluctuations and the level of agitation within the granular system; (c) it serves as an independent state variable and scales with the square of the shear rate under steady simple shearing. The granular temperature concept is also employed by the Granular Solid Hydrodynamics (GSH) framework (Jiang and Liu, 2009), it is defined at the mesoscopic particle scale, distinct from the conventional thermal temperature at the atomic scale. Note that the granular temperature from the GSH has a different structure compared to the kinetic theory (Luding et al., 2021).

By analogy, Wiebicke and Einav (2024) recently proposed a "clay temperature" to similarly characterize the kinetic energy of mesoscopic fluctuations in clay, extending this conceptual framework to fine-grained soils.

Appendix B. Stress and strain conditions in the simple shear test

Under the simple shear test, the second-order stress tensor is expressed as follows:

$$\boldsymbol{\sigma} = \begin{bmatrix} \sigma_{xx} & \tau_{xy} & 0 \\ \tau_{xy} & \sigma_{yy} & 0 \\ 0 & 0 & \sigma_{zz} \end{bmatrix} = \begin{bmatrix} \sigma_n & \tau & 0 \\ \tau & \sigma_n & 0 \\ 0 & 0 & \sigma_n \end{bmatrix} \tag{B1}$$

where σ_n is the vertical stress; τ is the shear stress.

Under the simple shear test, the second-order strain tensor is expressed as follows:

$$\boldsymbol{\varepsilon} = \begin{bmatrix} \varepsilon_{xx} & \varepsilon_{xy} & 0 \\ \varepsilon_{yx} & \varepsilon_{yy} & 0 \\ 0 & 0 & \varepsilon_{yy} \end{bmatrix} = \begin{bmatrix} \varepsilon_n & \frac{\gamma}{2} & 0 \\ \frac{\gamma}{2} & \varepsilon_n & 0 \\ 0 & 0 & \varepsilon_n \end{bmatrix} \tag{B2}$$

where ε_n is the vertical strain; γ is the shear strain, defined as the ratio of the horizontal displacement to sample height, i.e., $\gamma = \frac{\partial u}{\partial y}$.

Based on Eq.(B1), the hydrostatic and deviatoric stresses are express as:

$$p = \sigma_n \tag{B3}$$

$$q = \sqrt{3}\tau \tag{B4}$$

Based on Eq.(B2), the mean and deviatoric strains are express as:

$$\varepsilon_v = \varepsilon_n \tag{B5}$$

$$\varepsilon_d = \frac{|\gamma|}{\sqrt{3}} \tag{B6}$$

In the undrained simple test, the volumetric strain is zero, i.e., $\varepsilon_v = \varepsilon_n = 0$.

Appendix C. Formulations in kinetic-theory-based hydrodynamic model

1. Auxiliary functions for viscous mean stress p_v, shear viscosity η_v, and bulk viscosity γ_v

$$p_v = 4G(\Phi)F(\Phi, \varepsilon_n)\rho T_g \tag{C1}$$

$$\eta_v = \frac{8}{5\sqrt{\pi}}G(\Phi)J(\Phi, \varepsilon_n)\rho d T_g^{0.5} \tag{C2}$$

$$\gamma_v = \frac{4}{3\sqrt{\pi}}G(\Phi)Q(\Phi, \varepsilon_n)\rho d T_g^{0.5} \tag{C3}$$

where Φ is the volume fraction; ρ is the density; T_g is the granular temperature; d is the particle diameter; ε_n is the restitution coefficient; G, F, J, and Q are auxiliary functions related to the volume fraction (refer to Jenkins and Savage, 1983; Garzó and Dufty, 1999).

2. Stress equation under simple shear condition

Under simple shear conditions, the granular system reaches a steady state. By neglecting the divergence of the energy flux and assuming that all energy input from the work of the collisional stress is entirely dissipated through collisional mechanisms, the granular temperature can be derived. The granular temperature T_g is related to the square of the equivalent strain rate and particle diameter (see Feng and Yin (2025), for a detailed derivation), which is expressed as follows:

$$T_g \sim d^2\dot{\gamma}^2 \tag{C4}$$

where $\dot{\gamma}$ is the shear rate under simple shear conditions.

Based on the granular temperature, the shear viscosity and the viscous shear stress can be derived. For simplicity, only the primary scaling relationship is presented (see Eqs. (C5) and (C6)). These equations indicate that the viscosity of the sand increases with the shear rate under simple shear conditions, reflecting a shear-thickening behavior. Furthermore, the viscous shear stress is proportional to the square of the equivalent strain rate and the particle diameter.

$$\eta_g \sim \rho d T_g^{0.5} \sim \rho d^2\dot{\gamma} \tag{C5}$$

$$\tau_g \sim \rho d^2\dot{\gamma}^2 \tag{C6}$$

Data availability

The datasets generated during and/or analyzed during the current study are available from the corresponding author on reasonable request.

References

Bagnold, R.A., 1954. Experiments on a gravity-free dispersion of large solid spheres in a Newtonian fluid under shear. Proc. R. Soc. Lond. Ser. A Math. Phys. Sci. 225 (1160), 49–63.

Baumgarten, A.S., Kamrin, K., 2019. A general fluid–sediment mixture model and constitutive theory validated in many flow regimes. J. Fluid Mech. 861, 721–764.

Boukpeti, N., White, D.J., Randolph, M.F., Low, H.E., 2012. Strength of fine-grained soils at the solid–fluid transition. Géotechnique 62 (3), 213–226.

Chen, Y., 2020. A Viscoplastic Interpretation of Strain Rate Growth in Variably Saturated Soil Systems Subjected to Wetting. Doctoral dissertation. Northwestern University.

Cheng, W., Yin, Z.Y., 2024. Fractional order viscoplastic modeling of anisotropically overconsolidated clays with modified isotach viscosity. Int. J. Plast. 172, 103858.

Cotecchia, F., Guglielmi, S., Cafaro, F., Gens, A., 2019. Characterisation of the multi-scale fabric features of high plasticity clays. Géotechn. Lett. 9 (4), 361–368.

De Gennes, P.G., 1992. Soft matter. Science 256 (5056), 495–497.

Fall, A., Lemaitre, A., Bertrand, F., Bonn, D., Ovarlez, G., 2010. Shear thickening and migration in granular suspensions. Phys. Rev. Lett. 105 (26), 268303.

Feng, H., Yin, Z.Y., 2025. Enhanced elastoplasticity-based frictional-collisional model for solid–fluid phase transition of granular media. Comput. Geotech. 183, 107218.

Feng, H., Liang, W., Yin, Z.Y., Hu, L., 2025. Material point method modeling of granular flow considering phase transition from solid-like to fluid-like states. Int. J. Numer. Anal. Methods Geomech. 49 (6), 1642–1664.

Forterre, Y., Pouliquen, O., 2008. Flows of dense granular media. Annu. Rev. Fluid Mech. 40 (1), 1–24.

Garzó, V., Dufty, J.W., 1999. Dense fluid transport for inelastic hard spheres. Phys. Rev. E 59 (5), 5895.

GDR-MiDi, 2004. On dense granular flows. Eur. Phys. J. E 14, 341–365.

Goldhirsch, I., 2003. Rapid granular flows. Annu. Rev. Fluid Mech. 35 (1), 267–293.

Graham, J., Crooks, J., Bell, A.L., 1983. Time effects on the stress-strain behaviour of natural soft clays. Géotechnique 33 (3), 327–340.

Guglielmi, S., Cotecchia, F., Cafaro, F., Gens, A., 2024. Analysis of the micro to macro response of clays to compression. Géotechnique 74 (2), 134–154.

Hicher, P.Y., Wahyudi, H., Tessier, D., 2000. Microstructural analysis of inherent and induced anisotropy in clay. Mech. Cohes. Frict. Mater. 5 (5), 341–371.

Hill, R., 1958. A general theory of uniqueness and stability in elastic-plastic solids. J. Mech. Phys. Solids 6 (3), 236–249.

Jaeger, H.M., Nagel, S.R., Behringer, R.P., 1996. Granular solids, liquids, and gases. Rev. Mod. Phys. 68 (4), 1259.
Jenkins, J.T., Savage, S.B., 1983. A theory for the rapid flow of identical, smooth, nearly elastic, spherical particles. J. Fluid Mech. 130, 187–202.
Jiang, Y., Liu, M., 2009. Granular solid hydrodynamics. Granul. Matter 11 (3), 139–156.
Jop, P., Forterre, Y., Pouliquen, O., 2006. A constitutive law for dense granular flows. Nature 441 (7094), 727–730.
Lade, P.V., 2005. Overview of constitutive models for soils. In: Soil Constitutive Models: Evaluation, Selection, and Calibration, pp. 1–34.
Li, P., Shen, W., Hou, X., Li, T., 2019. Numerical simulation of the propagation process of a rapid flow-like landslide considering bed entrainment: a case study. Eng. Geol. 263, 105287.
Liu, A.J., Nagel, S.R., 1998. Jamming is not just cool any more. Nature 396 (6706), 21–22.
Liu, L.L., Zhang, P., Zhang, S.H., Li, J.Z., Huang, L., Cheng, Y.M., Wang, B., 2022. Efficient evaluation of run-out distance of slope failure under excavation. Eng. Geol. 306, 106751.
Liu, J., Li, S., Duan, G., 2023. Steady rheological behavior and unified strength model for reconstituted deep-sea sediments. Eng. Geol. 316, 107058.
Luding, S., Jiang, Y., Liu, M., 2021. Un-jamming due to energetic instability: statics to dynamics. Granul. Matter 23 (4), 80.
Lun, C.K.K., 2000. Numerical simulation of dilute turbulent gas–solid flows. Int. J. Multiphase Flow 26 (10), 1707–1736.
Meshkati, E., Talmon, A., Luger, D., Bezuijen, A., 2021. Rheology of Clay Rich Soft Sediments: From Fluid to Geo-Mechanics. Proc, Dredging Days.
Mitchell, J.K., Soga, K., 2005. Fundamentals of Soil Behavior, vol. 3. John Wiley & Sons, New York.
Prime, N., Dufour, F., Darve, F., 2014a. Unified model for geomaterial solid/fluid states and the transition in between. J. Eng. Mech. 140 (6), 04014031.
Prime, N., Dufour, F., Darve, F., 2014b. Solid-fluid transition modelling in geomaterials and application to a mudflow interacting with an obstacle. Int. J. Numer. Anal. Methods Geomech. 38 (13), 1341–1361.
Raz, T., Levine, R.D., 2023. The essence of phase transitions in condensed matter by an information theoretic approach. Proc. Natl. Acad. Sci. 120 (35), e2310281120.
Redaelli, I., Di Prisco, C., Vescovi, D., 2016. A visco-elasto-plastic model for granular materials under simple shear conditions. Int. J. Numer. Anal. Methods Geomech. 40 (1), 80–104.
Roy, S., Luding, S., Weinhart, T., 2017. A general (ized) local rheology for wet granular materials. New J. Phys. 19 (4), 043014.
Savage, S.B., 1998. Analyses of slow high-concentration flows of granular materials. J. Fluid Mech. 377, 1–26.
Schofield, A.N., Wroth, P., 1968. Critical State Soil Mechanics, Vol. 310. McGraw-hill, London.
Shen, W., Peng, J., Qiao, Z., Li, T., Li, P., Sun, X., Li, J., 2024. Plowing mechanism of rapid flow-like loess landslides: Insights from MPM modeling. Eng. Geol. 335, 107532.
Su, B., Li, Y., Han, Z., Ma, Y., Wang, W., Ruan, B., Tan, S., 2024. Topography-based and vectorized algorithm for extracting physical quantities in 3D-SPH form and its application in debris-flow entrainment modeling. Eng. Geol. 340, 107693.
Urmi, Z.A., Yerro, A., Saeidi, A., Chavali, R.V.P., 2024. Prediction of retrogressive landslide in sensitive clays by incorporating a novel strain softening law into the Material Point Method. Eng. Geol. 340, 107669.
Vescovi, D., Di Prisco, C., Berzi, D., 2013. From solid to granular gases: the steady state for granular materials. Int. J. Numer. Anal. Methods Geomech. 37 (17), 2937–2951.
Wang, D., Wang, X., Chen, X., Huang, Q., Wang, J., Lian, B., Wang, F., 2024. Solid–fluid phase transition characteristics of loess and its drag reduction mechanism. Landslides 21 (11), 2635–2653.
Wei, X., Li, J., Sun, Z., Xu, L., 2025. Study on the steady-state and dynamic rheological characteristics of five clayey materials. Constr. Build. Mater. 458, 139583.
Wiebicke, M., Einav, I., 2024. A simple hydrodynamic model for clay. J. Mech. Phys. Solids 192, 105789.
Wood, D.M., 1990. Soil Behaviour and Critical State Soil Mechanics. Cambridge University Press.
Wu, W., Wang, S., Alipour, M., 2020. Constitutive Modelling for Fast Granular Flow.
Xue, Y., Chen, N., Tang, R., Yang, Z., Jiao, M., Wen, T., Jin, J., 2025. Slope failure mechanism of the "5· 1" Meida Highway collapse in Guangdong, China: interaction between multi-source water and weathered granite soil. Landslides 22 (4), 1199–1212.
Yang, L., Zhang, M., Wang, L., Liu, T., Shi, P., Yin, B., Jiao, W., 2024. Failure kinematics and mechanisms of the 2019 Yahuokou flow-like landslide along the Pingding-Huama fault in Zhouqu segment. Eng. Geol. 332, 107448.
Ye, T., Jiang, Q., Zhang, C., Ma, Z., Li, C., 2024. High-speed long-runout landslide scraping and entrainment effects: a case study on Shuicheng landslide. Eng. Geol. 341, 107722.
Yi, J.T., Li, Y.P., Bai, S., Fu, Y., Lee, F.H., Zhang, X.Y., 2018. A simple effective stress approach for modeling rate-dependent strength of soft clay. J. Offshore Mech. Arct. Eng. 140 (4), 044501.
Yin, Z.Y., Hicher, P.Y., Jin, Y.F., 2020. Practice of Constitutive Modelling for Saturated Soils. Springer Nature.